Supplementary Information (SI) for Energy & Environmental Science.

Supplementary Information

Nature-inspired synergistic strategy: carrier regulation in breakdown self-healing all-organic polymer dielectrics for enhanced high-temperature energy storage

Wenjie Huang[a], Baoquan Wan[d], Wenye Zhang[a], Xing Yang[a], Zhonghua Xiang[b], Haobo Tian[e], Can Ding[e], Yiyi Zhang[f], Yong Chae Jung[g] and Jun-Wei Zha[a,b,c*]

[a]School of Chemistry and Biological Engineering, University of Science and Technology Beijing, Beijing 100083, P.R. China

[b]State Key Laboratory of Organic-Inorganic Composites, Beijing University of Chemical Technology, Beijing 100029, P.R. China

[c]State Key Laboratory of Alternate Electrical Power System with Renewable Energy Sources, School of Electrical and Electronic Engineering, North China Electric Power University, Beijing 102206, P.R. China

[d]State Key Laboratory of Power System Operation and Control, Department of Electrical Engineering, Tsinghua University, Beijing 100084, P.R. China

[e]School of Electrical Engineering and New Energy, China Three Gorges University, Hubei 443002, P.R. China

[f]School of Electrical Engineering, Guangxi University, Nanning 530004, P.R. China

[g]RAMP Convergence Research Center, Korea Institute of Science and Technology, Jeonllabuk-do 55324, Republic of Korea

[*]E-mail: zhajw@ncepu.edu.cn

Experimental

Materials

4,4'-(Hexafluoroisopropylidene)diphthalic anhydride and Dicyclohexyl-3,4,3',4'-tetracarboxylic dianhydride were supplied by China Tech (Tianjin) Chemical Co., Ltd. Diaminodicyclohexyl methane, 5'-phenyl-1,1':3',1"-terphenyl (PTP), tetraphenylmethane (TPM), 9,9′-spirobifluorene (SF), anhydrous ethanol and m-cresol were provided by Macklin reagent.

Synthesis and preparation

For FAPI and FAPI-based composite dielectrics, firstly, equimolar amounts of 4,4'-(Hexafluoroisopropylidene)diphthalic anhydride and Diaminodicyclohexyl methane were reacted in m-cresol solution at 90 °C for 4 h and 180 °C for 6 h in an N_2 atmosphere, and the FAPI prepolymers were precipitated in anhydrous ethanol and subsequently dried in a vacuum oven at 80 °C for 24 h. Subsequently, specific mass percentages (0, 0.5 wt%, 1.0 wt%, 1.5 wt%, and 2.0 wt%) of PTP/TPM/SF aromatic small molecules were incorporated into the FAPI prepolymers with a solid content of 10 wt%, respectively, and stirred at 60 °C for 6 h. The clear mixed solutions were cast on clean glass plates, which were sequentially passed through the following temperature procedures, i.e., 80 °C for 4 h, 100 °C, 150 °C, 200 °C for 1 h, respectively, and 250 °C for 2 h to evaporation the solvent and complete the imidization. Finally, FAPI and FAPI-based composite films, about 10 μm thickness, were peeled off in deionized water and dried in a vacuum oven at 80 °C for 12 h to evaporate water. For API and its composite films, API prepolymers were prepared by condensation polymerization of Dicyclohexyl-3,4,3',4'-tetracarboxylic dianhydride and Diaminodicyclohexyl methane, and other procedures were consistent with those for FAPI and FAPI-based composite films. In this work, FAPI/PTP, FAPI/TPM, and FAPI/SF represent FAPI with 1.5 wt% PTP, FAPI with 1.0 wt% TPM, and FAPI with 1.0 wt% SF, respectively, if not stated additionally.

Device preparation of stacked film capacitors

The electrode layers of the film capacitor were the Al foils with a thickness of about 10 μm. As shown in Fig. S44, the dielectric and electrode layers were distributed alternately, with the dielectric layer finally covering the top. Among them, the dielectric material was in the middle position, and each electrode layer was arranged in an alternating order of left and right, with a margin of 5 mm between the edges of the dielectric material and the electrodes to isolate the anode and cathode. The stacked multilayer blocks were hot pressed at 220 °C and a pressure of about 5 tons for 3 h and subsequently cooled to room temperature to obtain compact stacked multilayer films. The stacked film capacitors were prepared by leading Cu wires as outer electrodes to the two sides of the stacked multilayer films via conductive silver paste. In addition, the stacked multilayer film for observing the interfacial structure of the electrode layer and the dielectric layer was an Al foil as a substrate, and then the Al foil layer and the dielectric material layer were constructed layer by layer, and finally capped with the Al foil layer, and the rest of the process was consistent with the above.

Characterization

Fourier transform infrared (FTIR) spectra of FAPI and FAPI-based composite dielectrics from 600 cm^{-1} to 4000 cm^{-1} were measured by a Nicolet-6700 instrument with attenuated total reflection mode. The ^{1}H NMR spectroscopy of FAPI was measured on a Bruker Avance III HD 500 MHz spectrometer using deuterated chloroform as solvent. Gel permeation chromatography (GPC) test was performed in tetrahydrofuran solution at 35 °C with an elution rate of 1.0 mL min^{-1} on a Waters-E2695 GPC system equipped with a refractive index detector. The apparent molecular weights were determined using polystyrene as standards. X-ray diffraction patterns were performed with a PANalytical X'Pert PRO (Cu Kα, $\lambda = 1.5418$ Å) instrument. The ultraviolet-visible absorption spectra were recorded on a Shimadzu UV-1800 spectrophotometer. Differential scanning calorimetry were performed in a DSC Q2000 instrument to obtain the glass transition temperature. Dynamic thermo-mechanical analysis (DMA) curves for obtaining the modulus were determined by a Hitachi DMA7100 instrument. Thermogravimetric analysis was carried out by a thermogravimetric analyser (Mettler Toledo TGA), recording from 30 °C to 600 °C with a heating rate of 10 °C min^{-1} under a nitrogen atmosphere. Scanning electron microscope morphology and EDS elemental mapping were examined by a Hitachi SU8010 microscope, and optical microscope images were characterized with AOSVI optical instrument to observe the surface morphology of the metallized films after electrical breakdown. Thermogravimetric analyzer (TG 209 F1 Libra®) and FTIR spectrometer

(Thermo Scientific Nicolet iS5) were combined to investigate gas-phase products of samples at high temperatures. The space charge density and electric field strength distributions of the films were determined by the HY-PEA-DPT01 test system and the samples polarized at 70 °C and 30 MV m^{-1} for 20 min. Thermally stimulated depolarization current (TSDC) were recorded by a Huace TSDC-3000 test system. The samples were polarized at 200 °C and 20 MV m^{-1} for 20 min. Subsequently, the polarized sample was fast cooled to 10 °C for 3 minutes. Afterwards, the samples were short-circuited and heated to 240 °C at a rate of 3 °C min^{-1} and the current was recorded. In the dielectric properties and TSDC tests, the electrode diameter of the samples was 20 mm. The electrical breakdown strength of the film samples was evaluated using a BOHER HV 72030P voltage withstand instrument. Displacement-Electric Field (*D*-*E*) loops under a unipolar wave at 100 Hz and leakage currents were recorded using a radiation-precision multiferroics test system. In the breakdown strength, leakage current density and *D*-*E* loops tests, the electrode diameter of the samples was 4 mm. The dielectric properties of samples were measured using a Novocontrol Concept 40 Broadband Dielectric Spectrometer. The capacitance properties of film capacitor devices were determined by the TH-2839 precision impedance analyzer.

Density functional theory (DFT) calculation

DFT calculations for the ground state geometry optimizations of the FAPI structure unit, PTP, TPM, and SF aromatic small molecules were performed on the Gaussian 09W program with the B3LYP/6-31G(d) basis set and functional[1-3]. Quantitative calculations of the surface electrostatic potential of the molecular model were conducted with the Multiwfn (V3.7) program with a grid spacing and electron density of 0.25 bohr and 0.001 e $bohr^{-3}$[4, 5]. Reduced density gradient (RDG) scatter plots of FAPI and FAPI/SF were analyzed by Multiwfn program. The iso-surfaces of non-covalent interactions was plotted by Multiwfn combined with visual molecular dynamics (VMD) programs[6]. The energies were calculated based on the WB97XD/6-31G(d,p) basis set and functional for the optimized electronic structures of FAPI structural units, SF small molecule, and the composite system of FAPI structural units and SF small molecule. To more accurately analyze the interaction energies, Basis Set superposition error (BSSE) corrections were performed using the counterpoise correction method. Thus, the interaction between the FAPI polymer and the aromatic small molecule can be expressed as: $E_{interaction} = E_{AB} - E_A - E_B + E_{BSSE}$. The PM6 semi-empirical method was employed for structure optimization to rapidly determine the system energies corresponding to specific dihedral angles of aromatic small molecules at different rotation angles.[7] Furthermore, TDDFT calculations based on CAM-B3LYP/6-31G(d) basis set and functional were conducted to investigate the excited state electron transition of FAPI structural unit, PTP, TPM, and SF aromatic small molecules[8, 9]. Further, the effects of varying the electric field strength along the x-axis direction on the electronic transition energies of the FAPI structural unit, PTP, TPM, and SF aromatic small molecules were calculated for electric fields ranging from 0 to 2.4×10^{-3} a.u. (0~1234 MV/m).

Molecular dynamics (MD) simulations

Polymer molecular chains with a polymerization degree of 25 were constructed in Material Studio software, and amorphous cells containing four molecular chains with an initial density of 0.2 g cm^{-3} were constructed by the Amorphous Cell module, and the components (PTP, TPM, and SF) were introduced separately. The amorphous cells were subjected to five rounds of annealing simulations from 298 K to 698 K in a normal pressure and temperature (NPT) system with a total annealing duration of 800 ps, Andersen thermostat, and Berendsen pressostat. Then, the amorphous cells were subjected to relaxation in the NPT system for 1000 ps at 298K and 0.0001 GPa, with Nose thermostat and Berendsen pressostat. The density of the model after relaxation was 1.259 g cm^{-3}, close to the real density. Finally, to further equilibrate the model adequately, molecular dynamics simulations were performed in a normal volume and temperature (NVT) system for 1000 ps. The molecular dynamics time step for each stage was 1 fs, and the electrostatic interaction was analyzed by the PPPM algorithm and the Compass III force field. The model was annealed and molecular dynamics simulated to obtain a reasonable polymer configuration, and the free and occupied volumes and densities of the polymer system were further calculated.

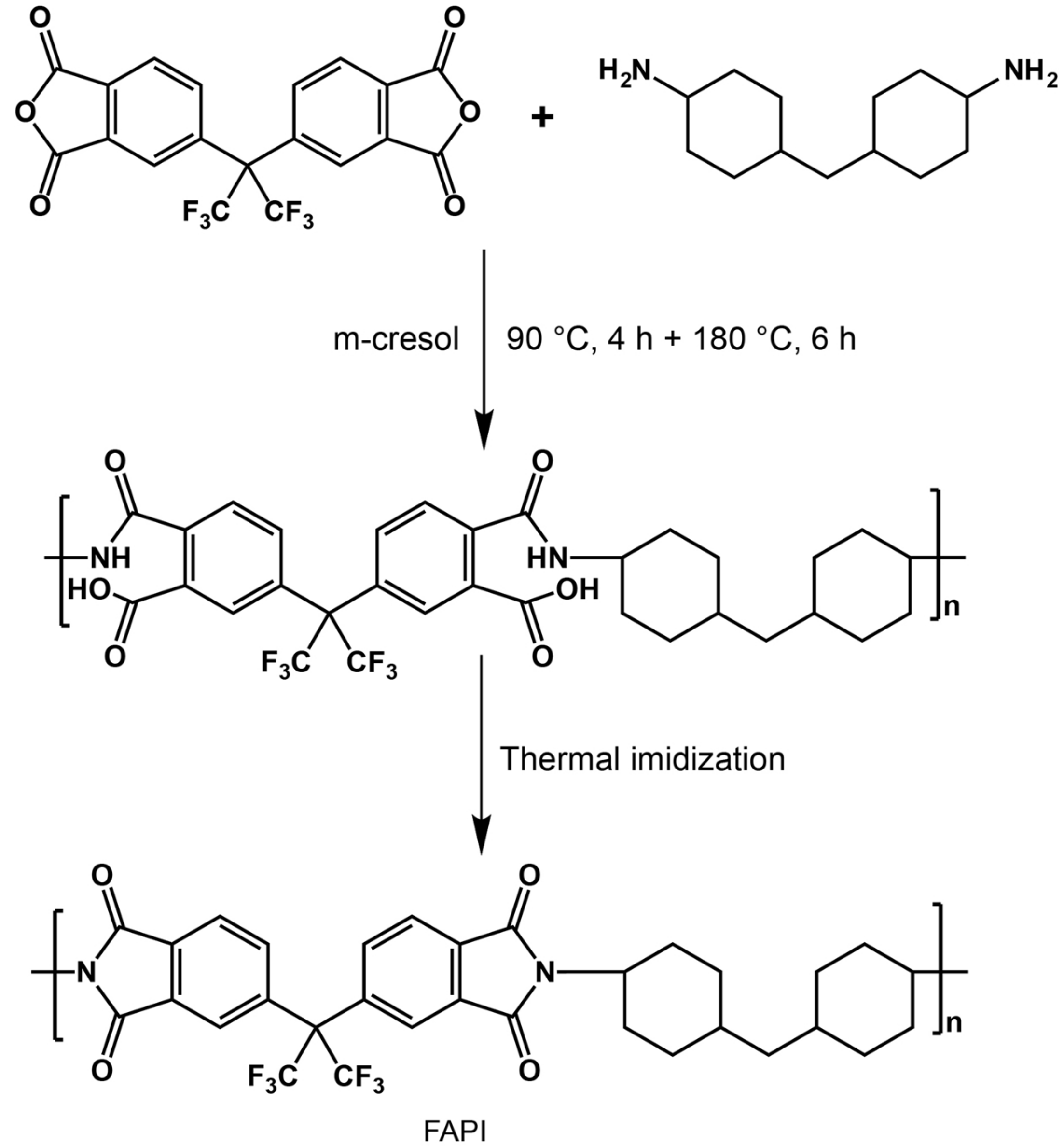

Fig. S1 Synthesis process of FAPI.

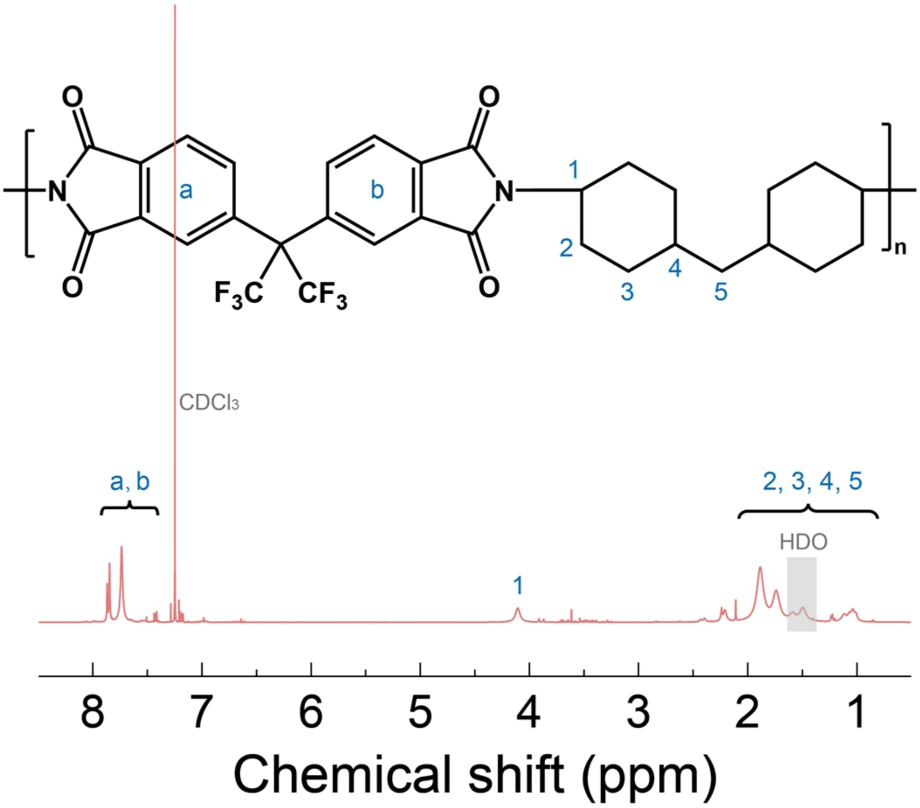

Fig. S2 ^{1}H NMR spectroscopy of FAPI.

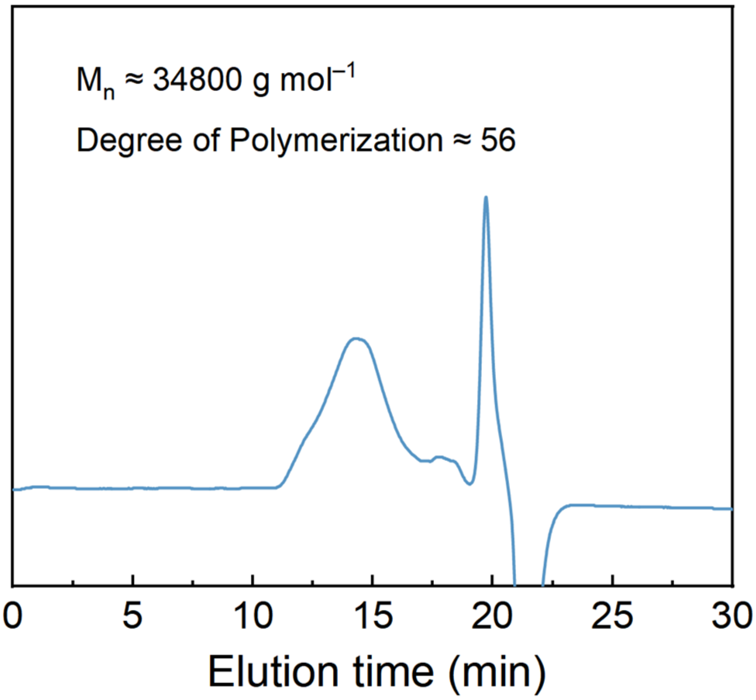

Fig. S3 GPC trace of FAPI polymer.

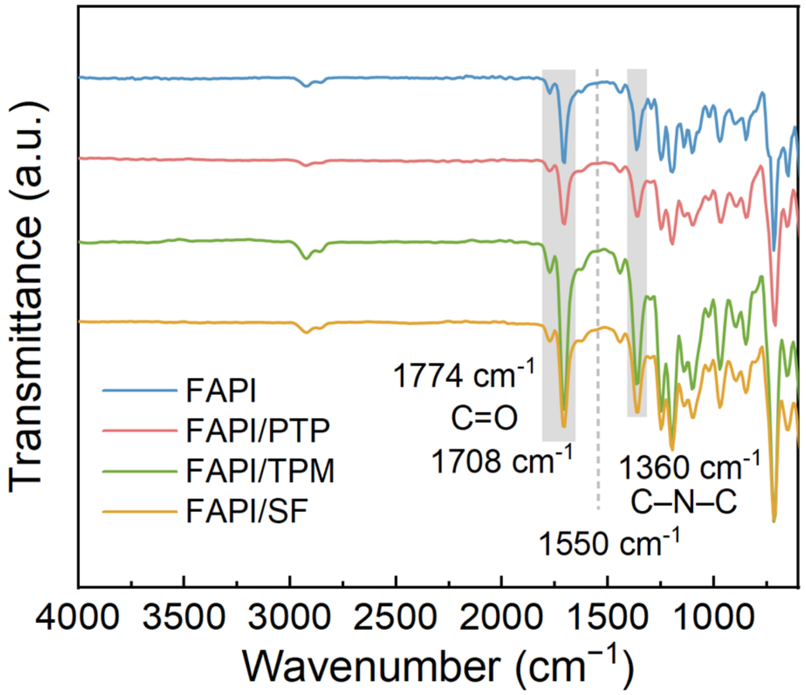

Fig. S4 FTIR spectroscopy of FAPI and FAPI-based composite dielectrics.

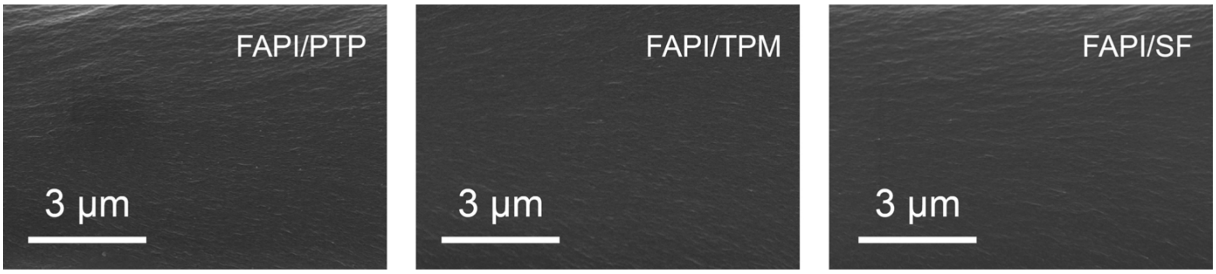

Fig. S5 The cross-sectional morphology of FAPI-based composite films.

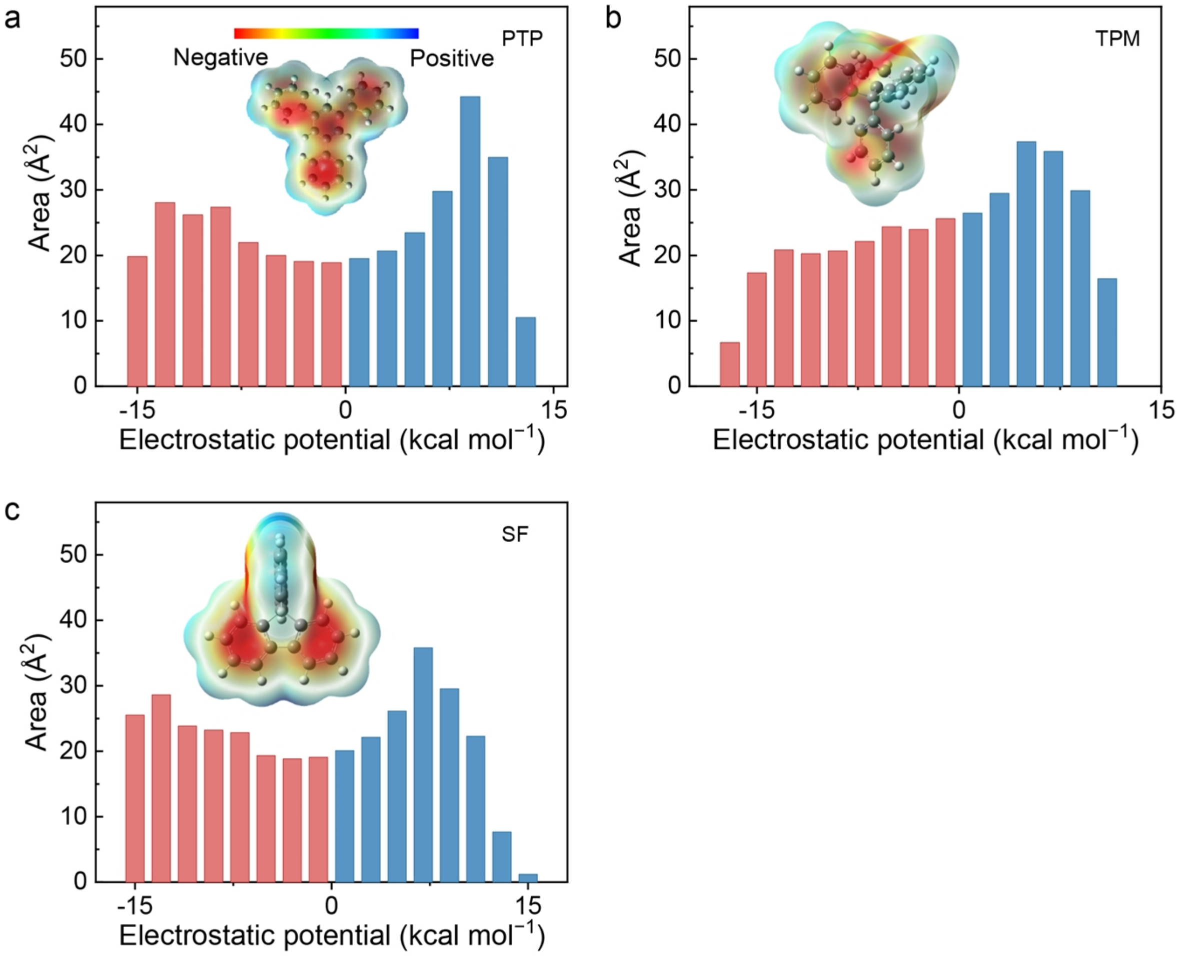

Fig. S6 Quantitative analysis of the surface electrostatic potential of (a) PTP, (b) TPM, and (c) SF aromatic small molecules.

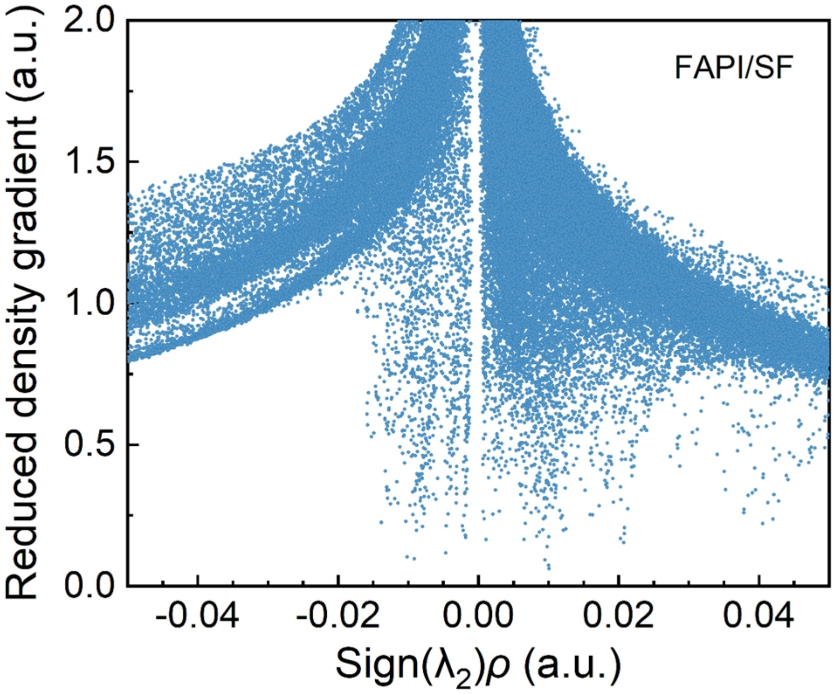

Fig. S7 Reduced Density Gradient scatter plots for FAPI/SF.

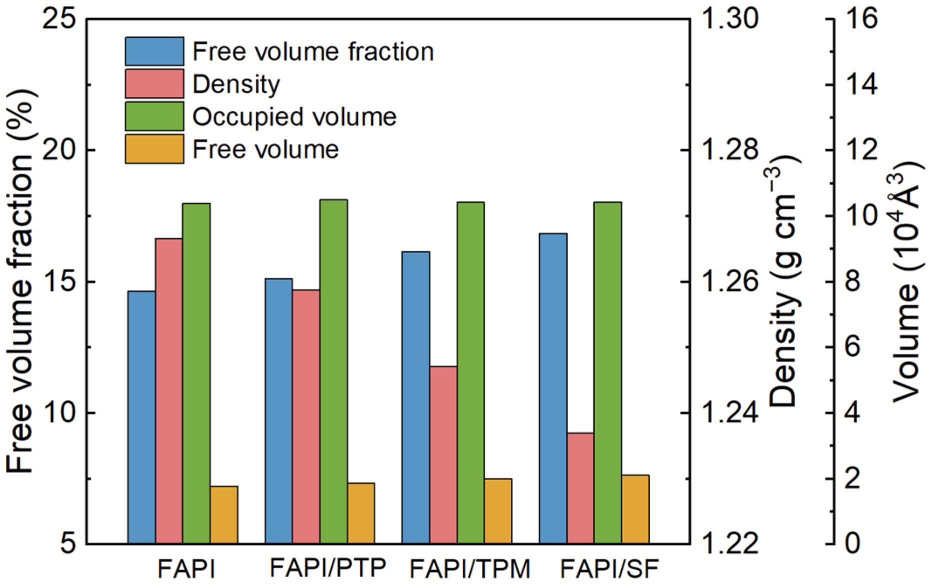

Fig. S8 Free volume fraction, free volume, unoccupied volume and density of FAPI and FAPI-based composite dielectrics simulated by molecular dynamics.

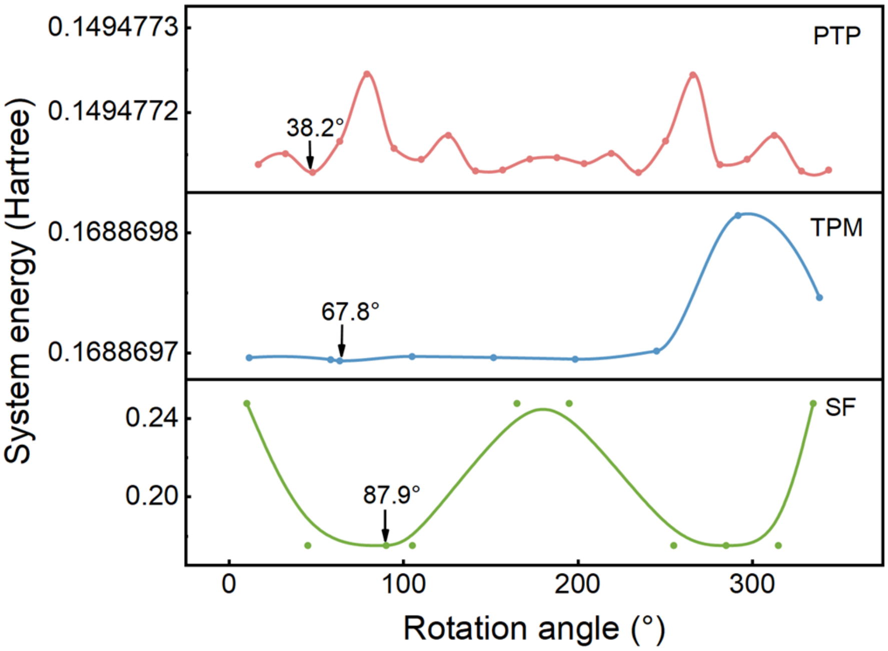

Fig. S9 Relationship between the dihedral angle of specific benzene ring units and molecule energy.

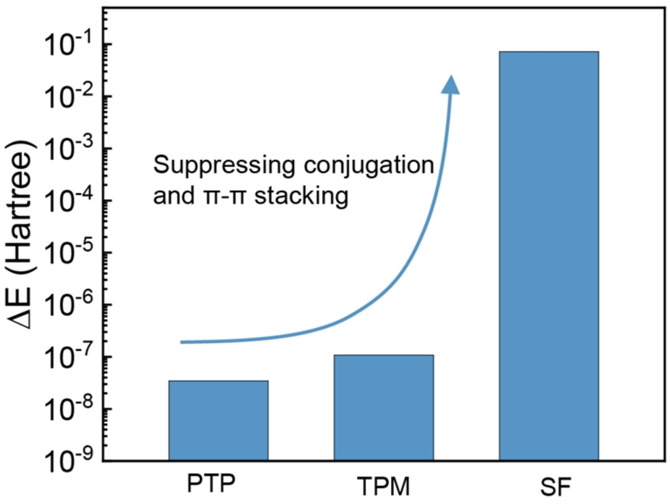

Fig. S10 Maximum rotational energy barriers for dihedral angles of specific benzene ring units corresponding to aromatic small molecules.

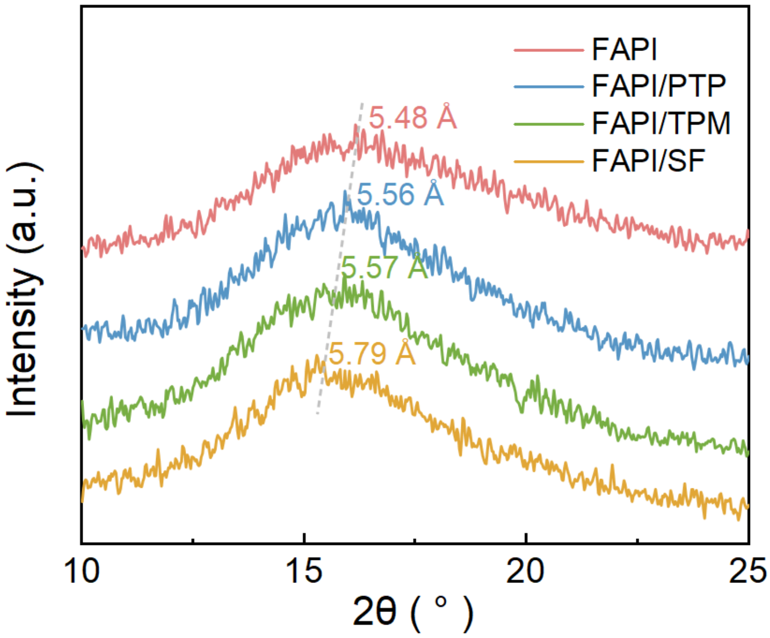

Fig. S11 XRD patterns of FAPI and FAPI-based composite dielectrics.

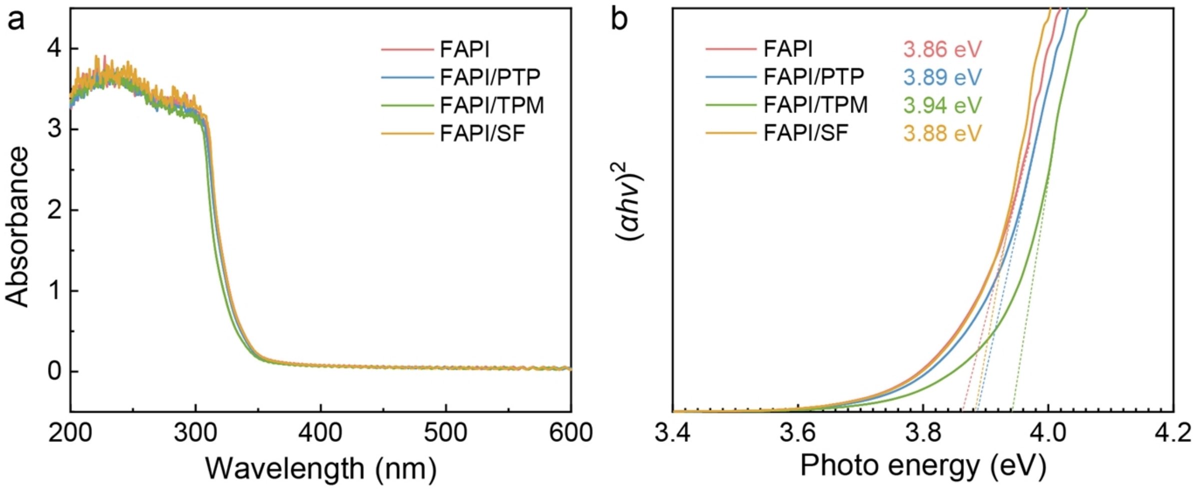

Fig. S12 (a) UV-Vis spectra and (b) Tauc plots of FAPI and FAPI-based composite dielectrics.

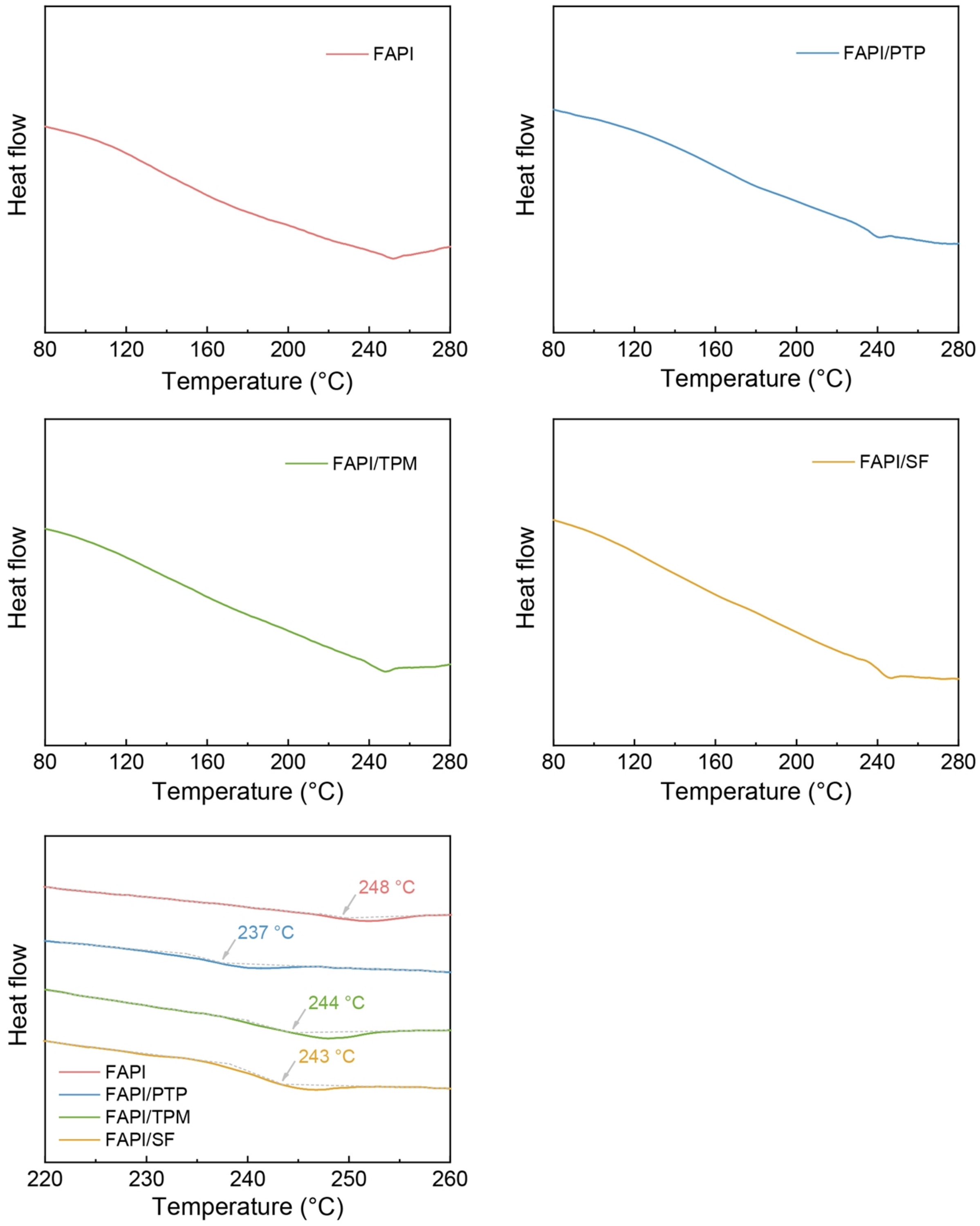

Fig. S13 DSC curves of FAPI and FAPI-based composite dielectrics.

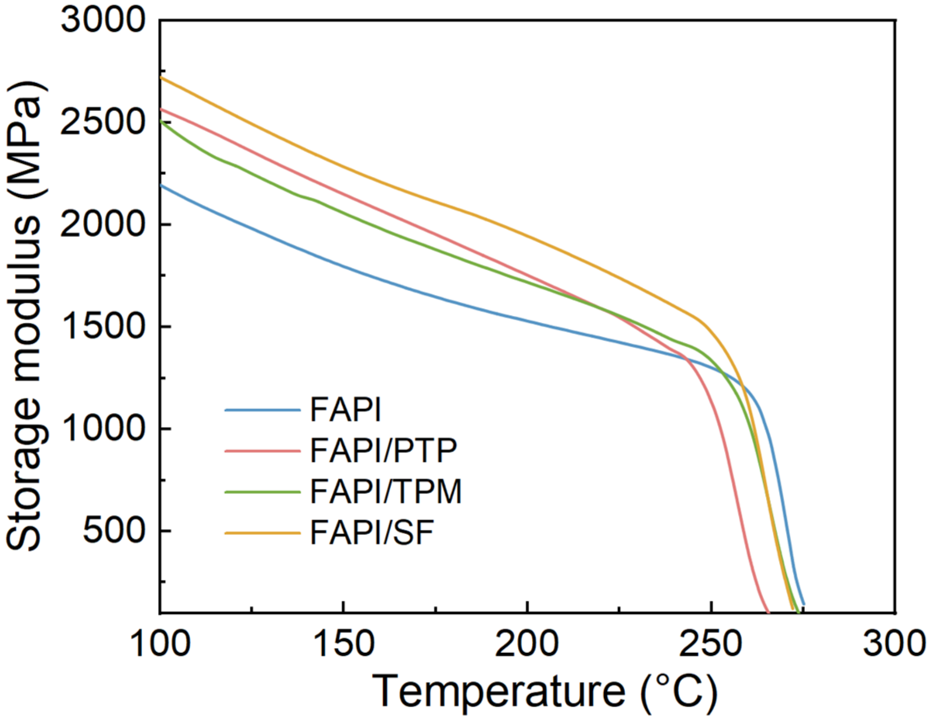

Fig. S14 DMA curves of FAPI and FAPI-based composite dielectrics.

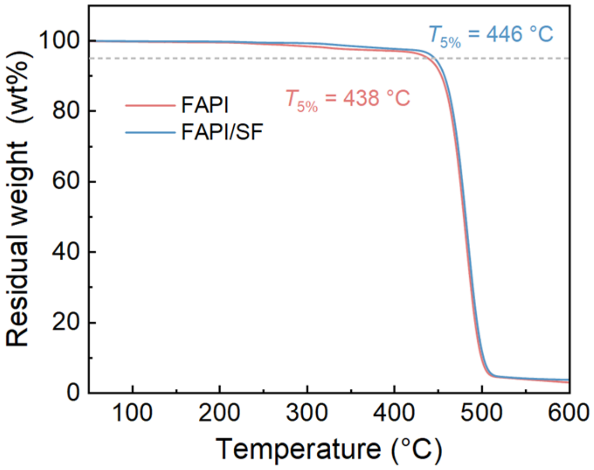

Fig. S15 TGA curves of FAPI and FAP/SF dielectrics.

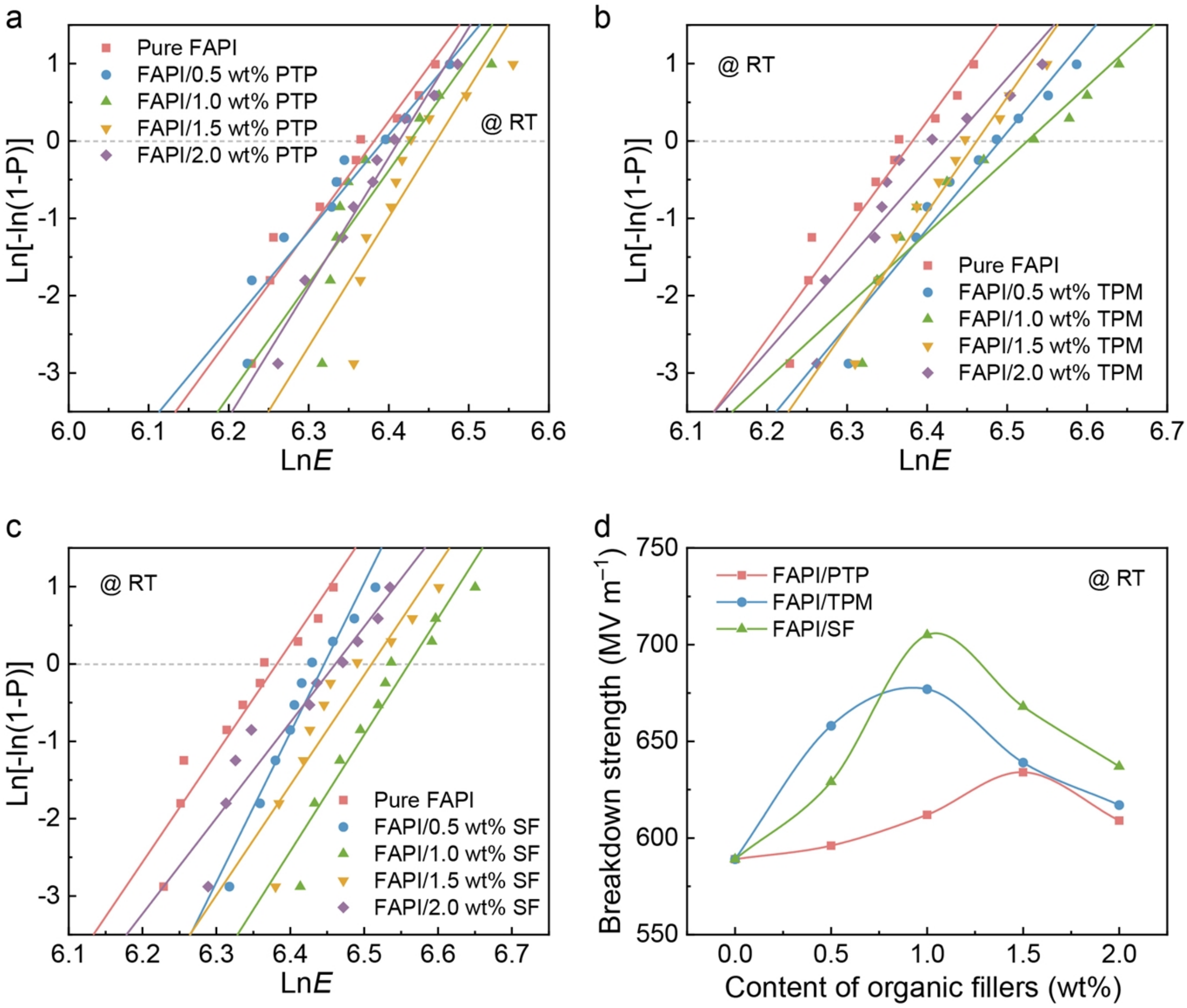

Fig. S16 Weibull breakdown strengths of (a) FAPI/PTP, (b) FAPI/TPM, and (c) FAPI/SF composite films with different aromatic small molecule contents, and (d) the E_b versus filler content of FAPI/PTP, FAPI/TPM, and FAPI/SF films at room temperature.

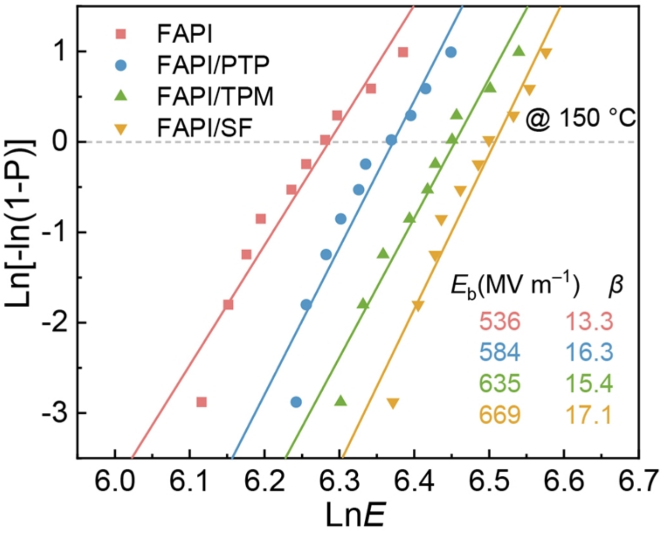

Fig. S17 Breakdown strength of FAPI and FAPI-based composite dielectrics at 150 °C.

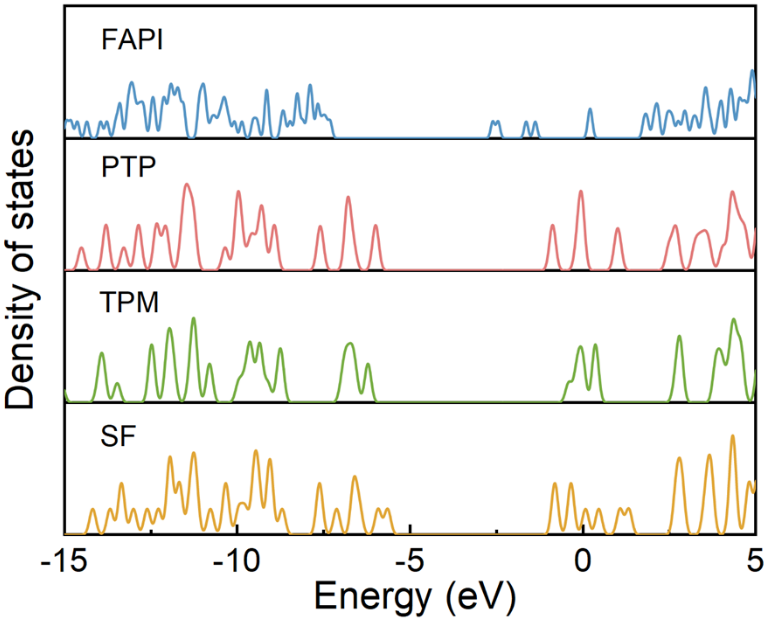

Fig. S18 Density of states for FAPI structural units and aromatic small molecules simulated by DFT.

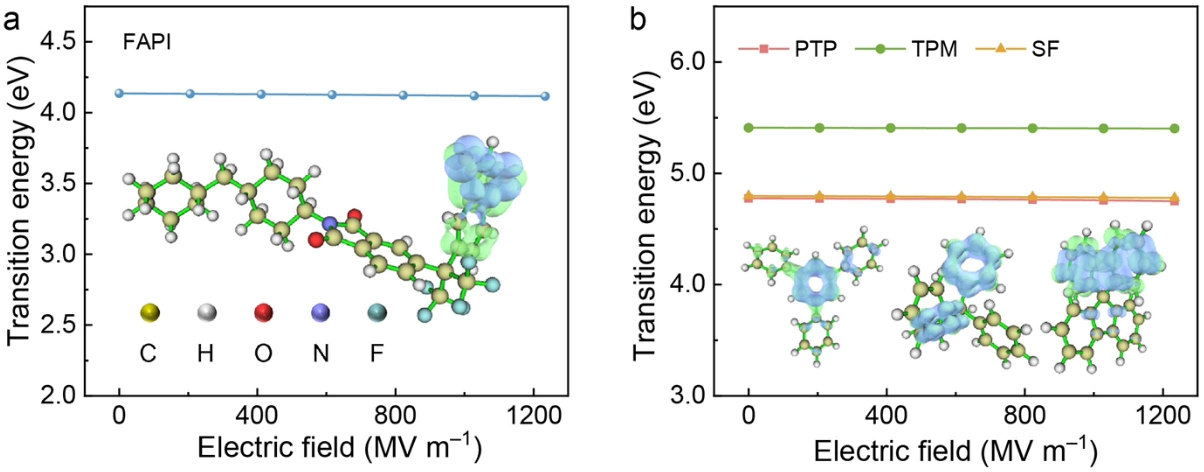

Fig. S19 DFT simulations of the electronic transition energies of (a) FAPI structural units and (b) aromatic small molecules under applied electric fields.

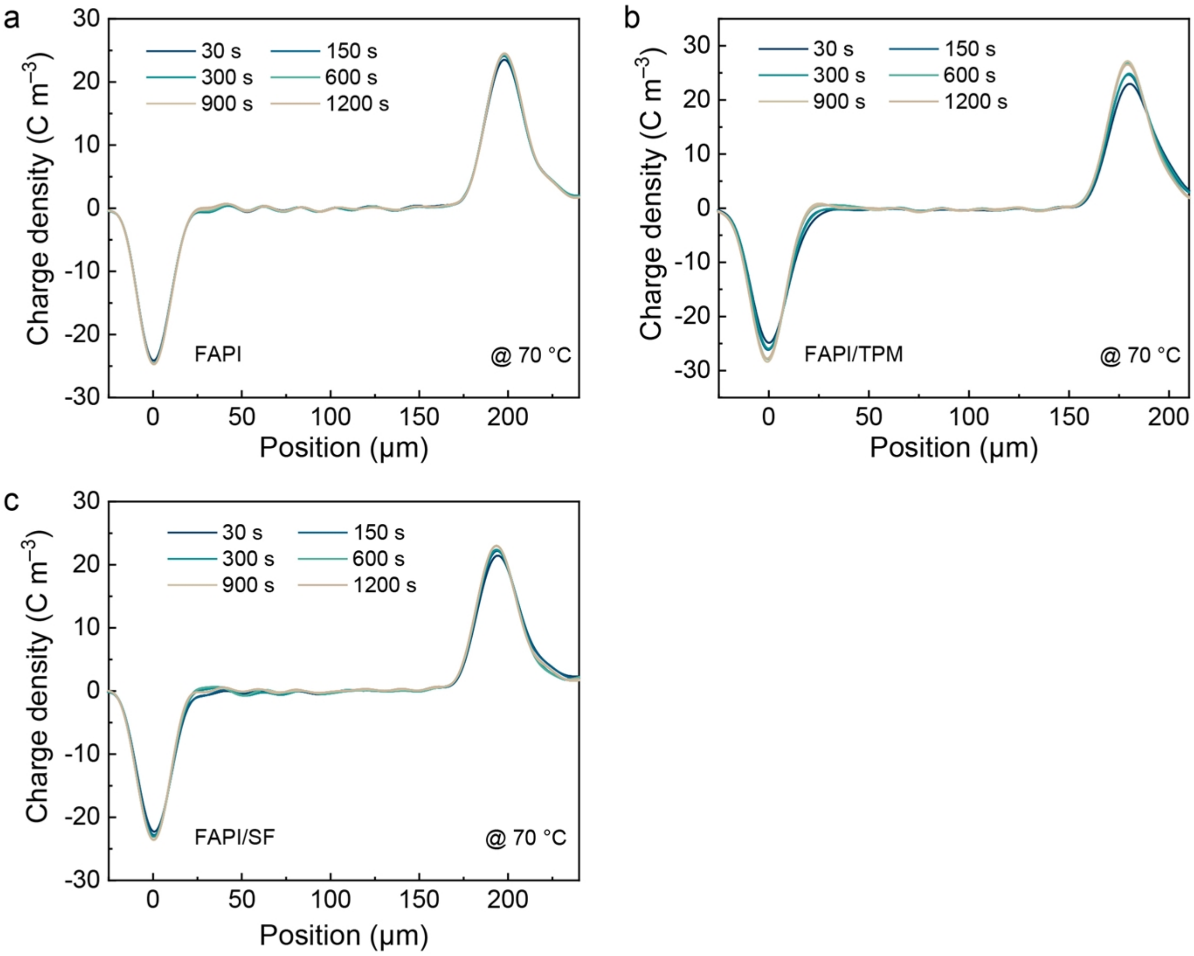

Fig. S20 Space charge density curves of (a) FAPI, (b) FAPI/TPM, and (c) FAPI/SF under an applied electric field.

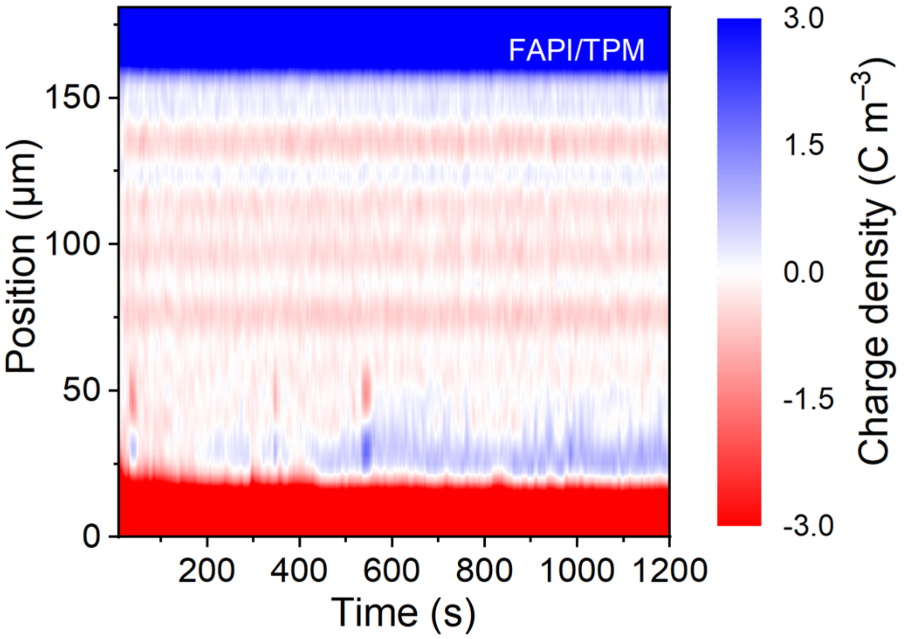

Fig. S21 Space charge density distributions of FAPI/TPM under an applied electric field.

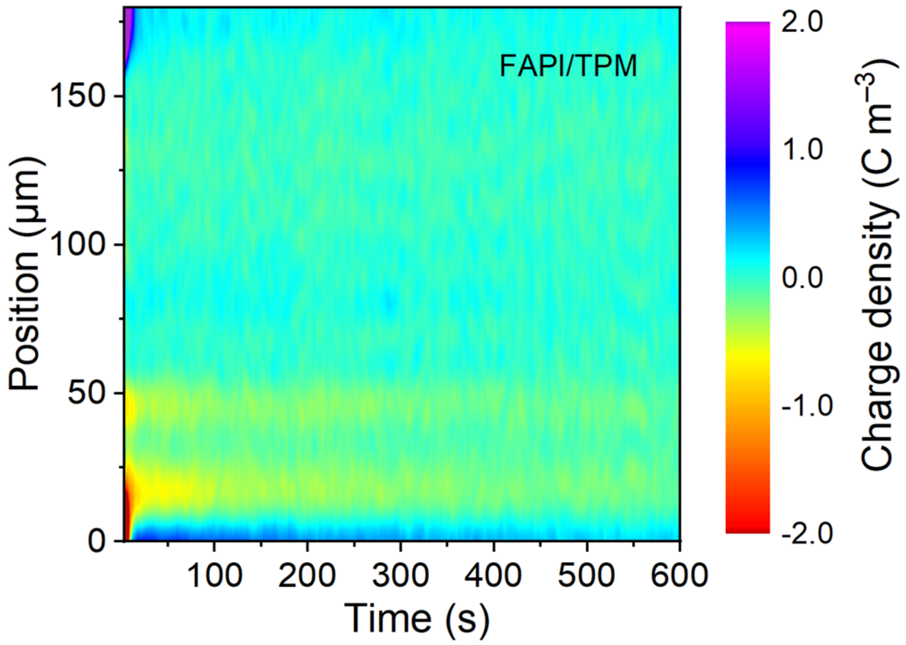

Fig. S22 Space charge density distributions of FAPI/TPM after removing the electric field.

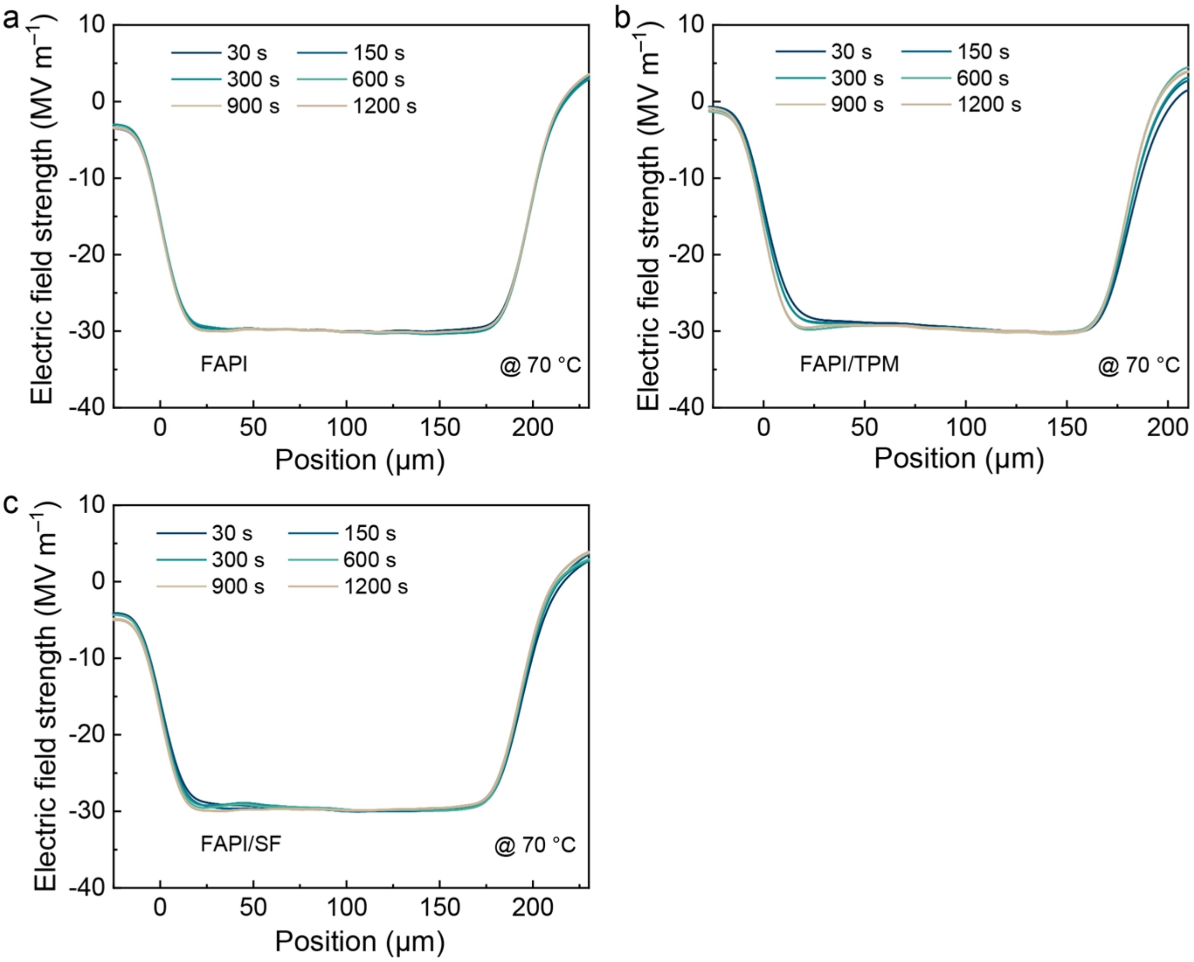

Fig. S23 Electric field strength curves of (a) FAPI, (b) FAPI/TPM, and (c) FAPI/SF under an applied electric field.

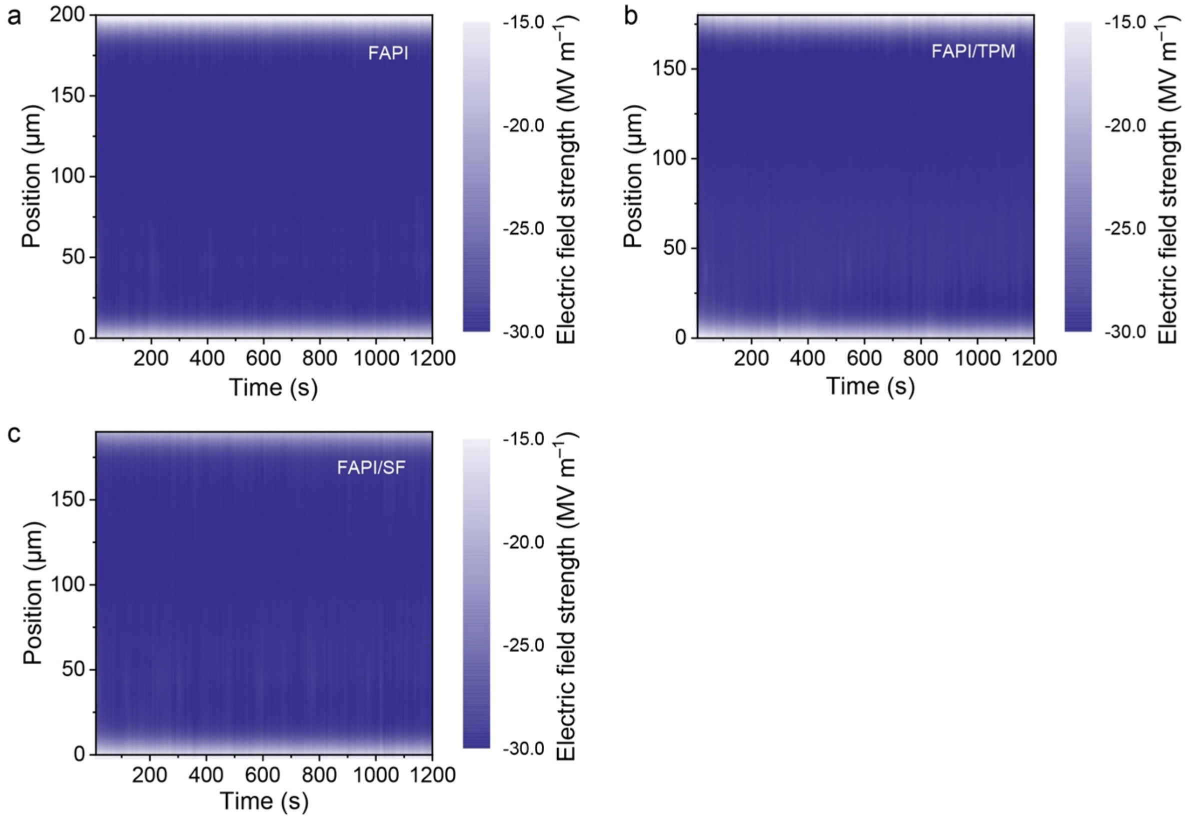

Fig. S24 Electric field strength distribution of (a) FAPI, (b) FAPI/TPM, and (c) FAPI/SF under an applied electric field.

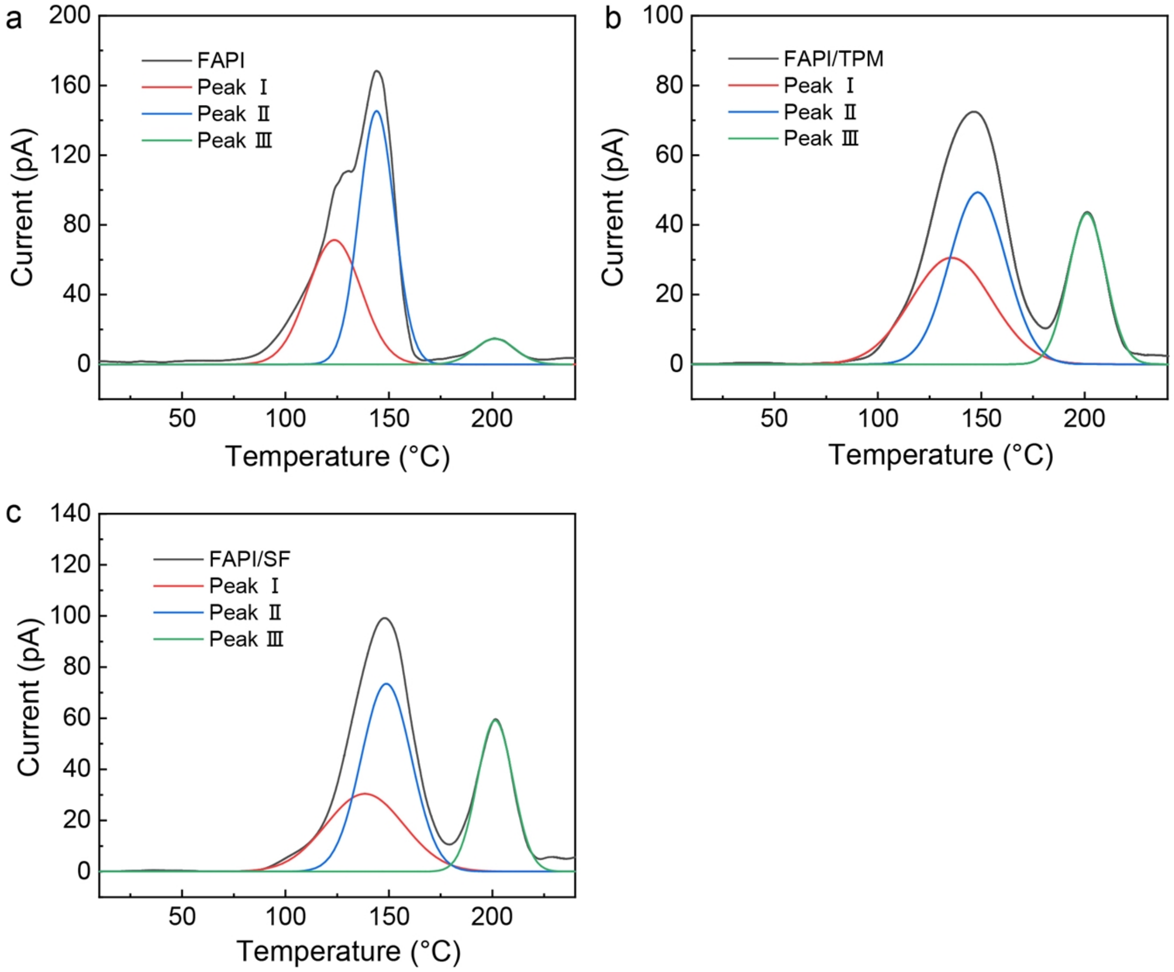

Fig. S25 TSDC curves of (a) FAPI, (b) FAPI/TPM, and (c) FAPI/SF.

Table S1 Trap depth and trapped charge quantity of FAPI and FAPI-based composite dielectrics.

	β-relaxation (Peak I) (°C)	Shallow trap (Peak II)		Deep trap (Peak III)	
		Trap depth (eV)	Trapped charge quantity (nC)	Trap depth (eV)	Trapped charge quantity (nC)
FAPI	123.6	1.84	62.3	2.10	7.13
FAPI/TPM	135.6	1.18	33.8	2.24	19.7
FAPI/SF	138.4	1.33	44.7	2.36	25.5

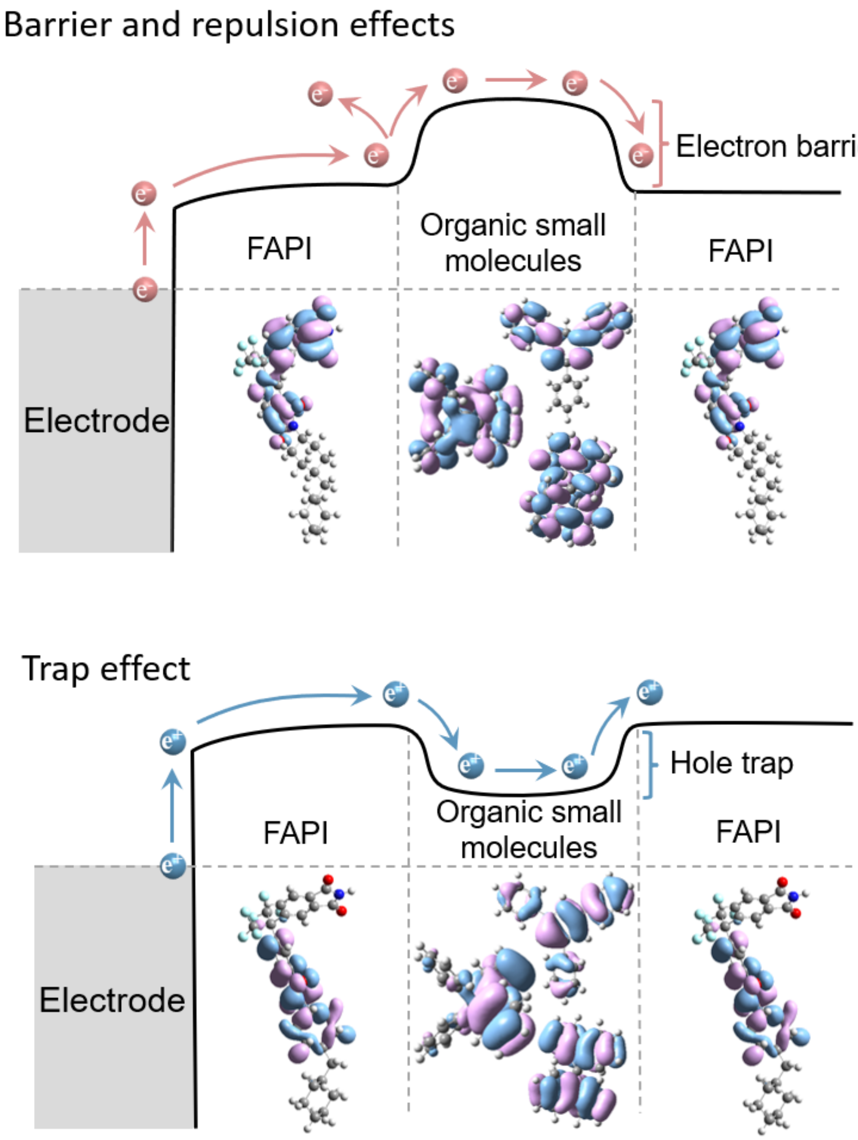

Fig. S26 Schematic diagram of carrier barrier, repulsion and trap effects constructed by aromatic small molecules in composites.

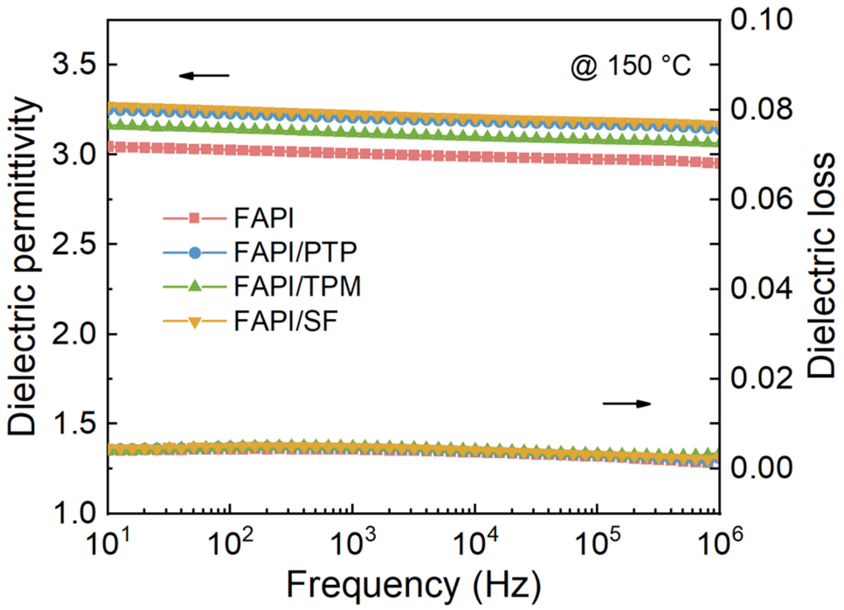

Fig. S27 Frequency-dependence of dielectric properties of FAPI and FAPI-based composite dielectrics at 150 °C.

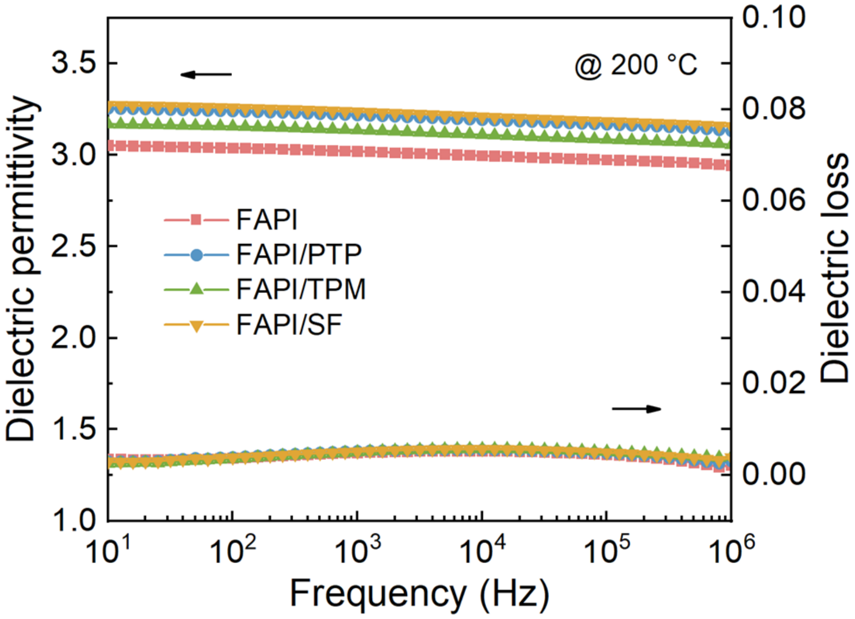

Fig. S28 Frequency-dependence of dielectric properties of FAPI and FAPI-based composite dielectrics at 200 °C.

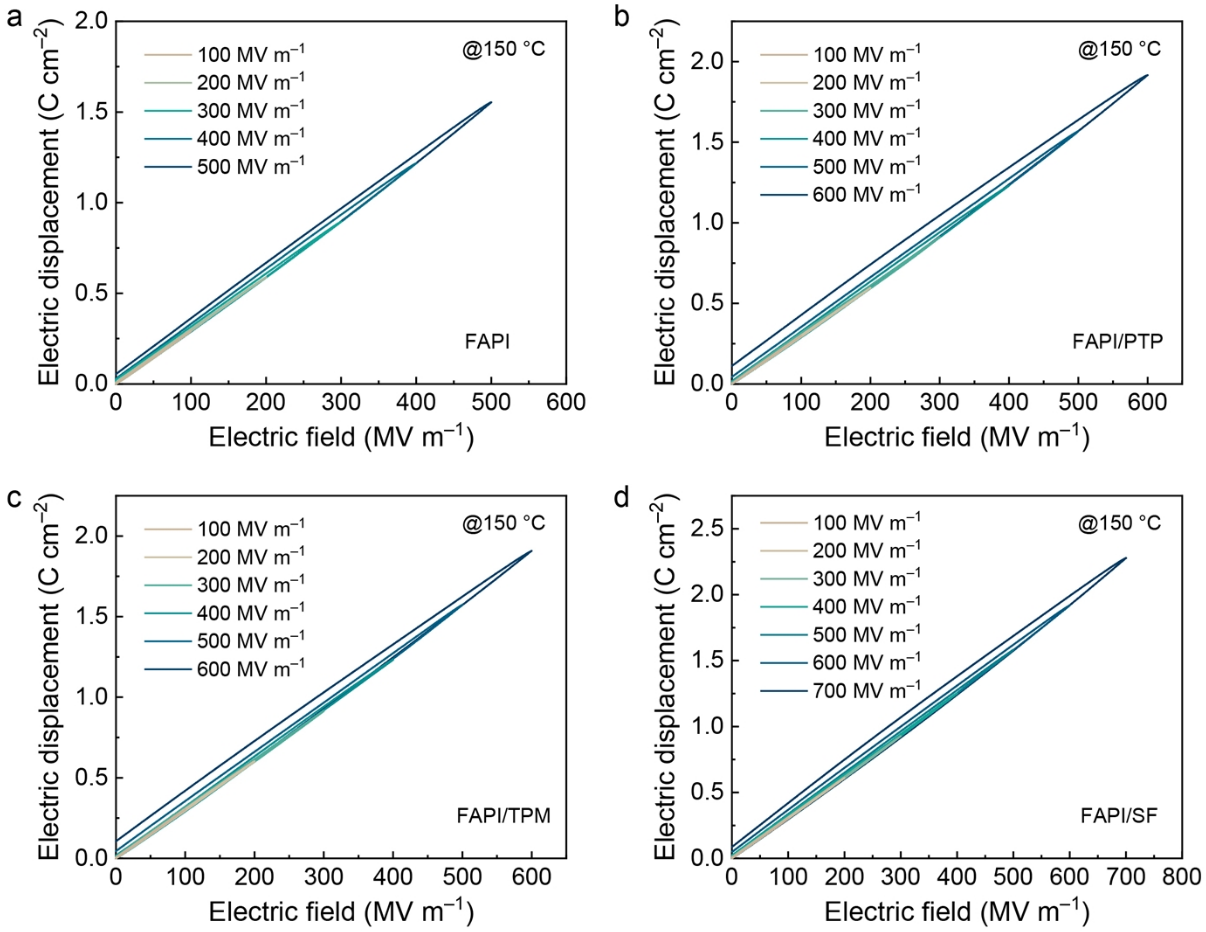

Fig. S29 Unipolar *D-E* loops of (a) FAPI film, (b) FAPI/PTP, (c) FAPI/TPM, and (d) FAPI/SF composite films at 150 °C with 100 Hz.

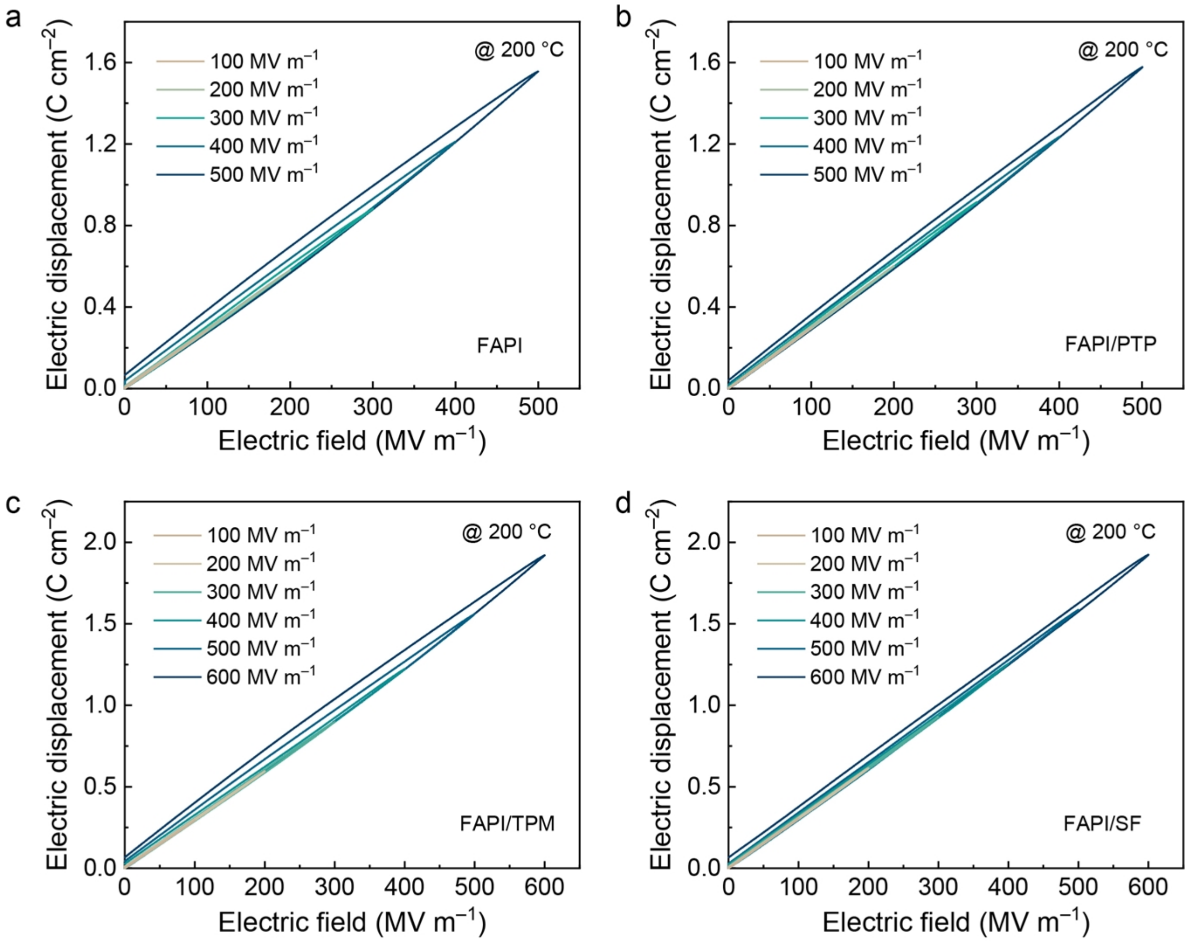

Fig. S30 Unipolar *D*-*E* loops of (a) FAPI film, (b) FAPI/PTP, (c) FAPI/TPM, and (d) FAPI/SF composite films at 200 °C with 100 Hz.

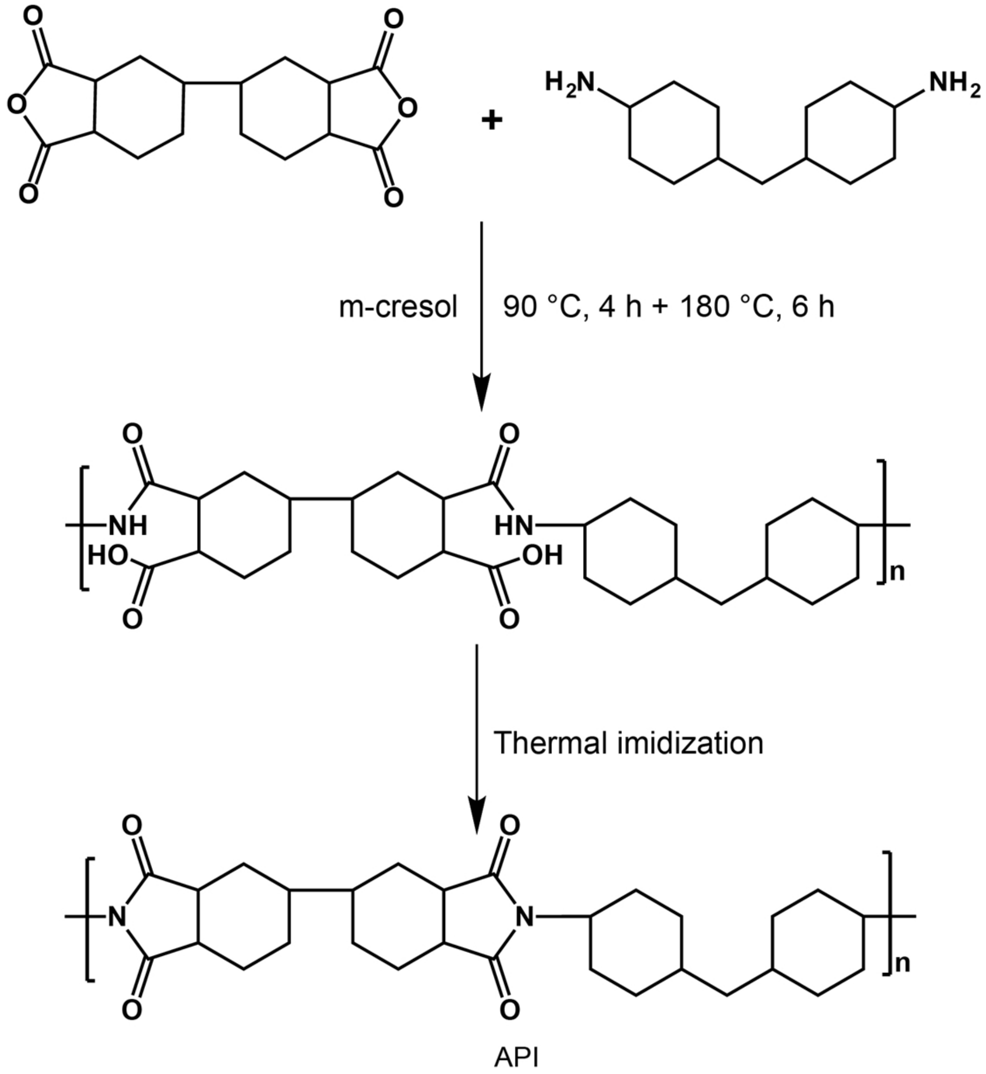

Fig. S31 Synthesis process of API.

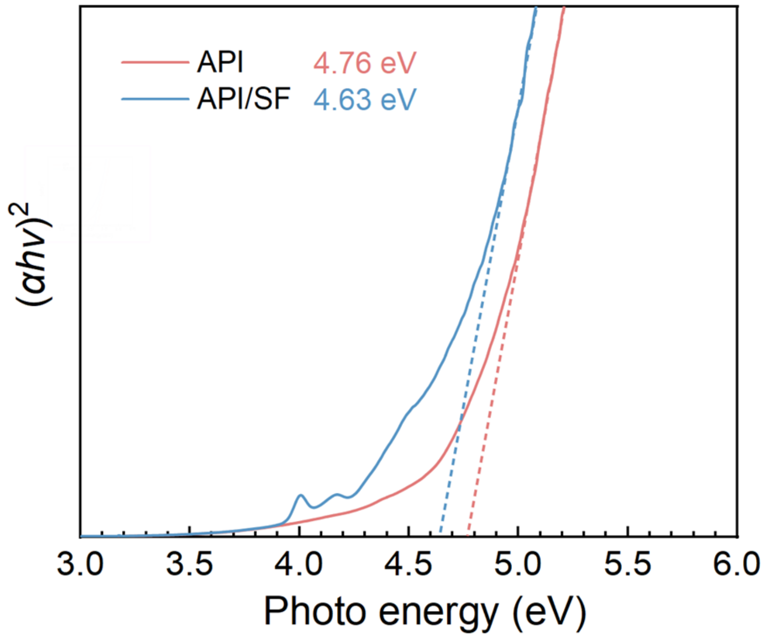

Fig. S32 Tauc plots of API film and API/SF composite film.

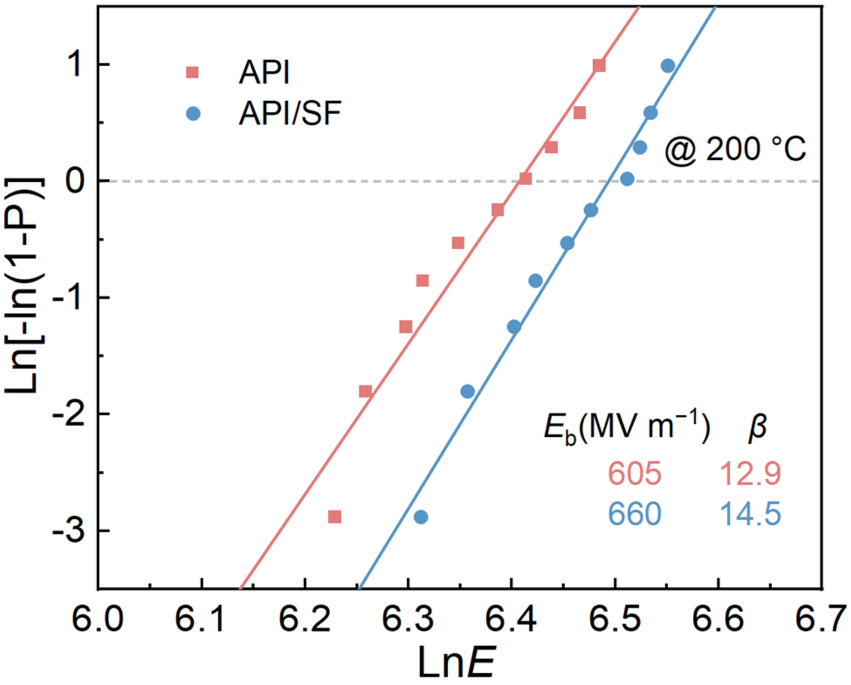

Fig. S33 Breakdown strength of API film and API/SF composite film at 200 °C.

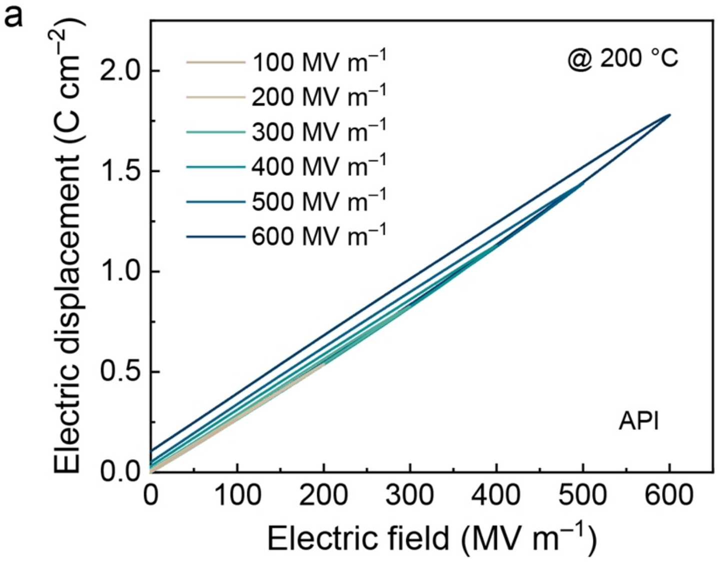

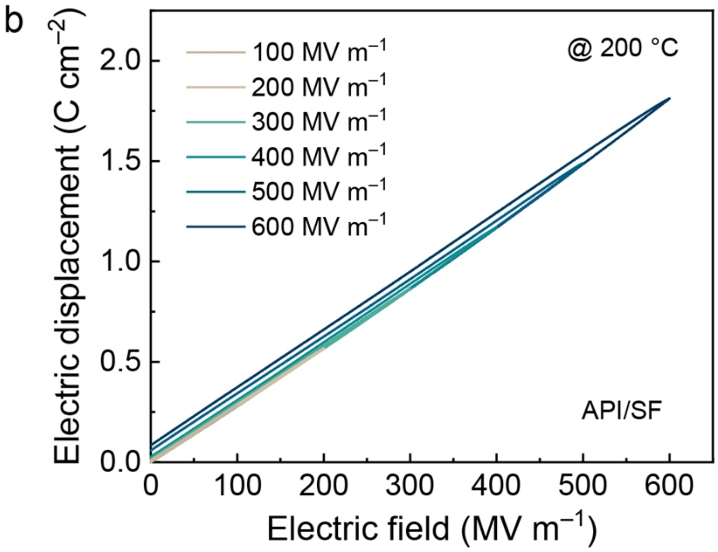

Fig. S34 Unipolar *D-E* loops of (a) API film and (b) API/SF composite film at 200 °C with 100 Hz.

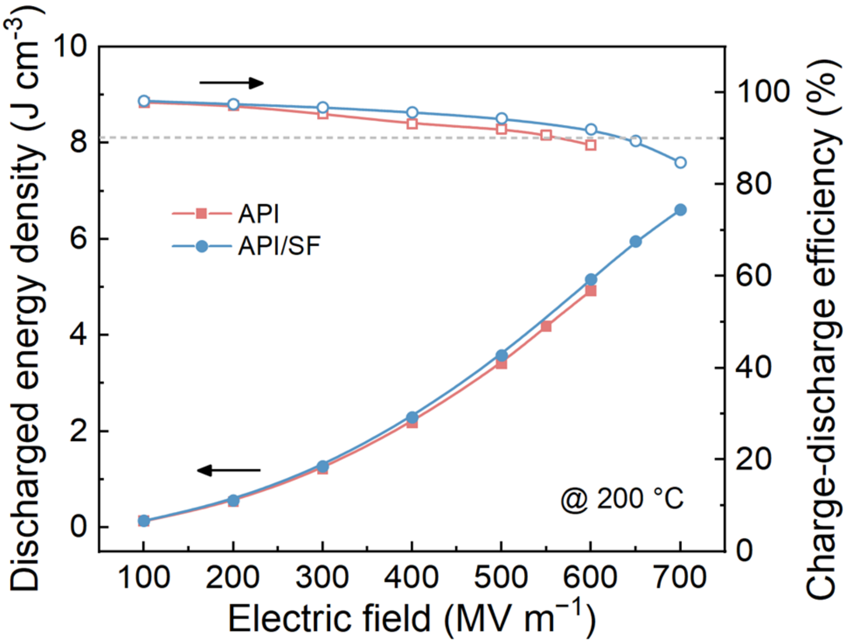

Fig. S35 Energy storage properties of API film and API/SF composite film at 200 °C.

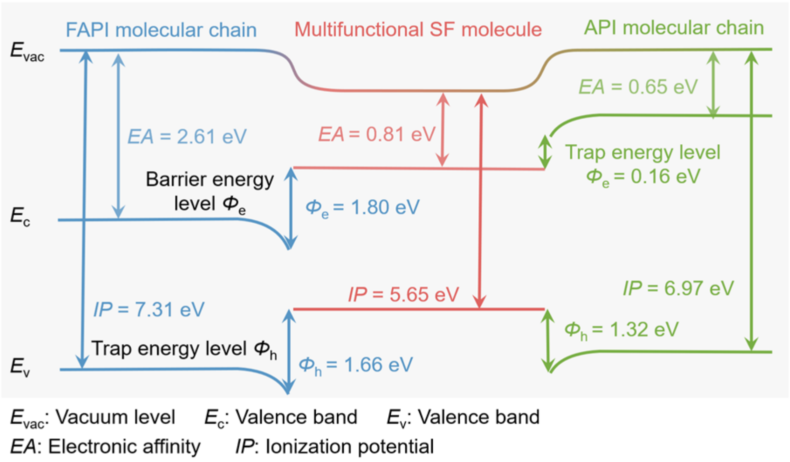

Fig. S36 Molecular orbital energy level structures of FAPI structural units, SF small molecules and API structural units.

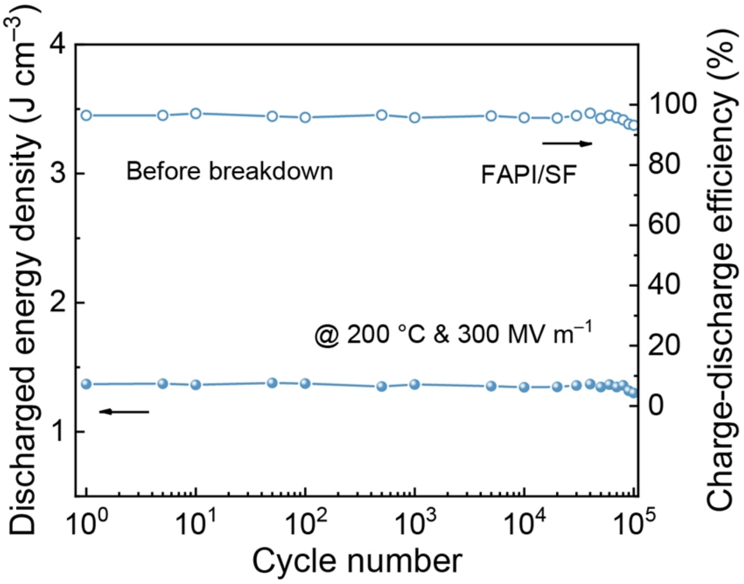

Fig. S37 Charge-discharge cycling stability of FAPI/SF composite film at 200 °C and 300 MV m^{-1}.

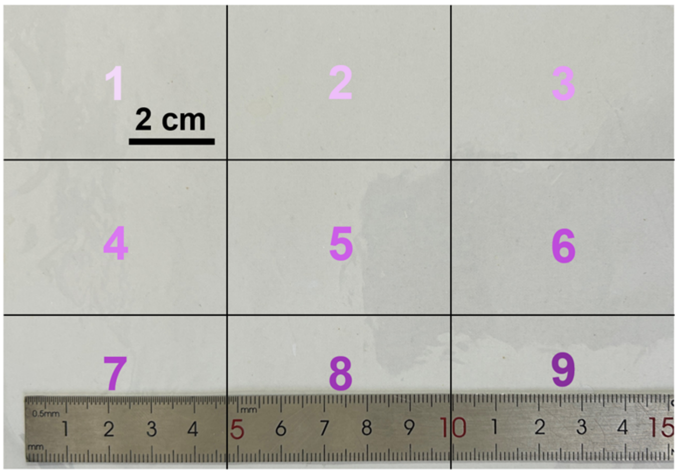

Fig. S38 Photograph of a large-scale FAPI/SF composite film.

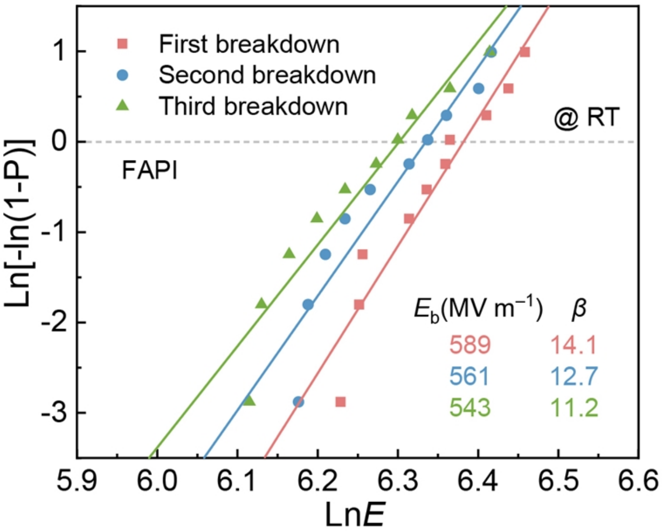

Fig. S39 Multiple electrical breakdown strength of FAPI film.

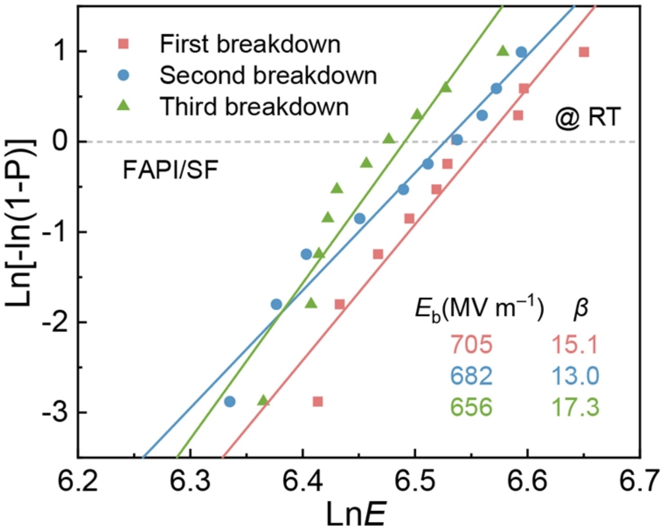

Fig. S40 Multiple electrical breakdown strength of FAPI/SF composite film.

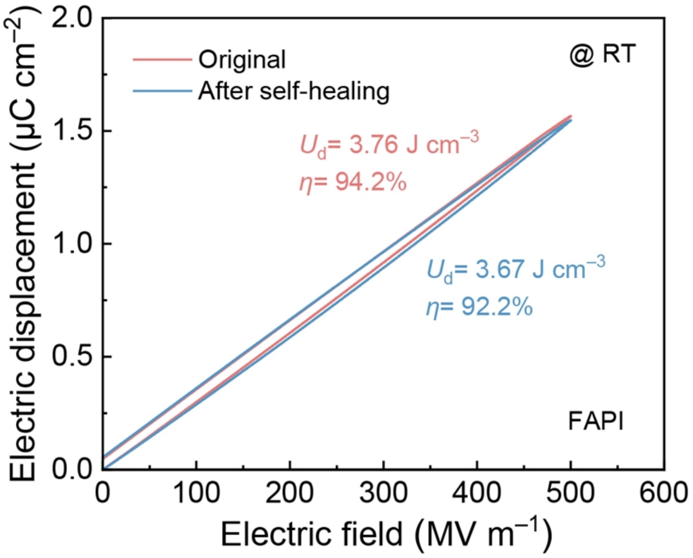

Fig. S41 *D-E* loops of FAPI film before and after electrical breakdown self-healing.

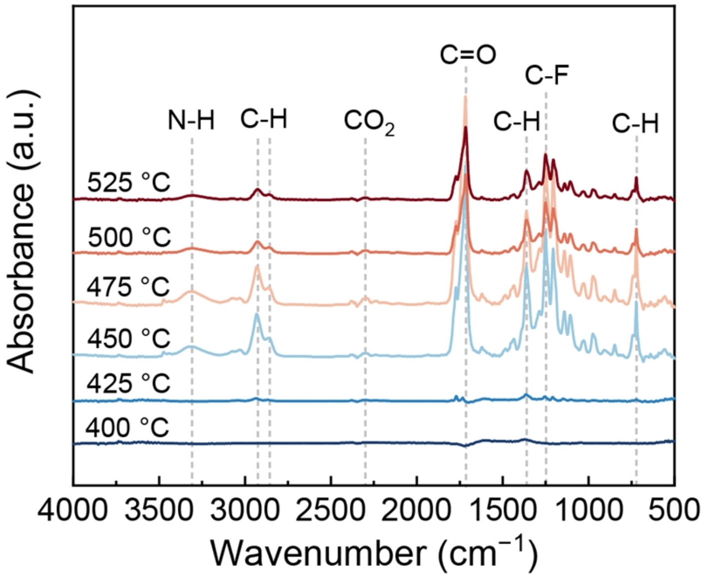

Fig. S42 FTIR spectroscopy of FAPI/SF composite film at different thermal decomposition temperatures.

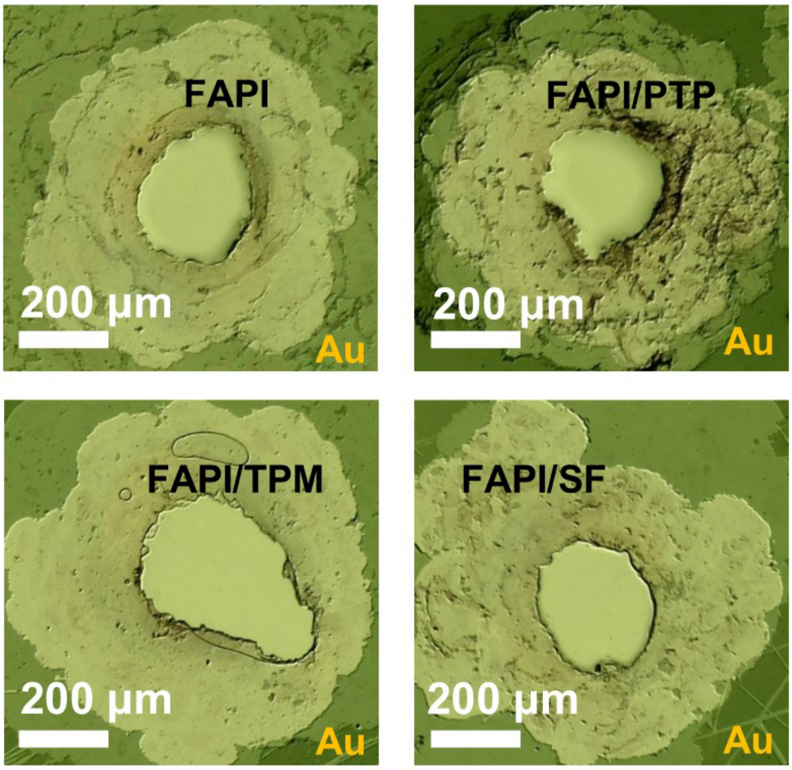

Fig. S43 Optical microscopic morphology of FAPI and FAPI-based composite films after electrical breakdown self-healing.

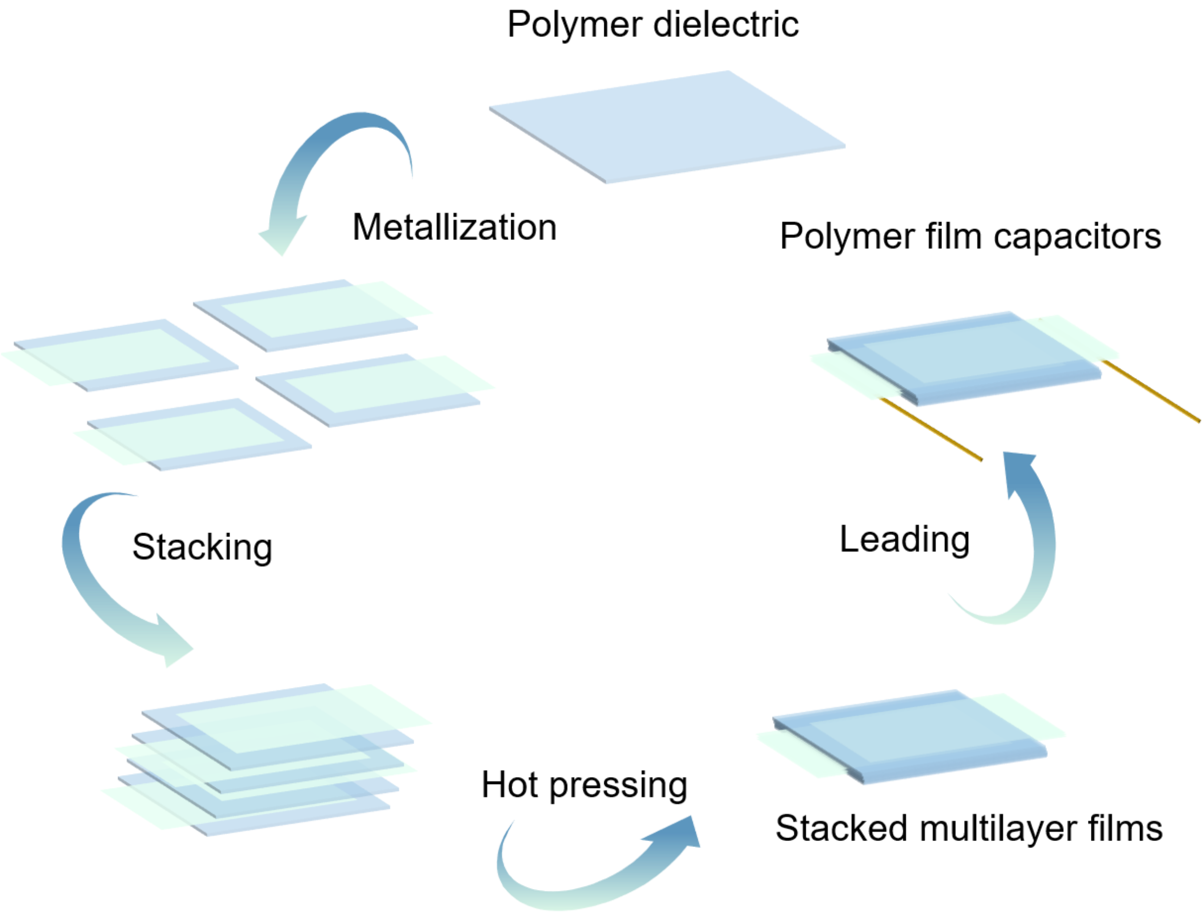

Fig. S44 Schematic diagram of fabrication process for polymer stacked film capacitor device.

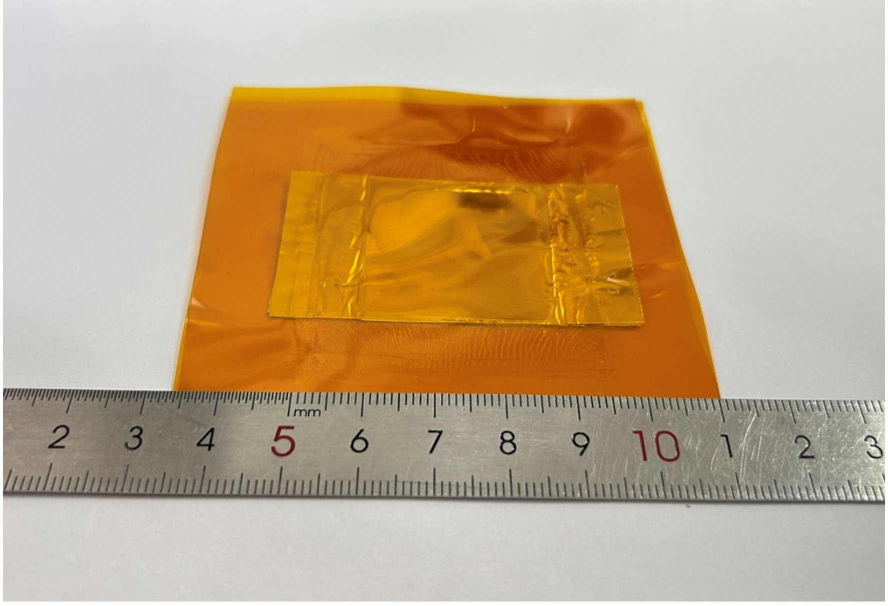

Fig. S45 Photograph of metallized stacked films after hot pressing.

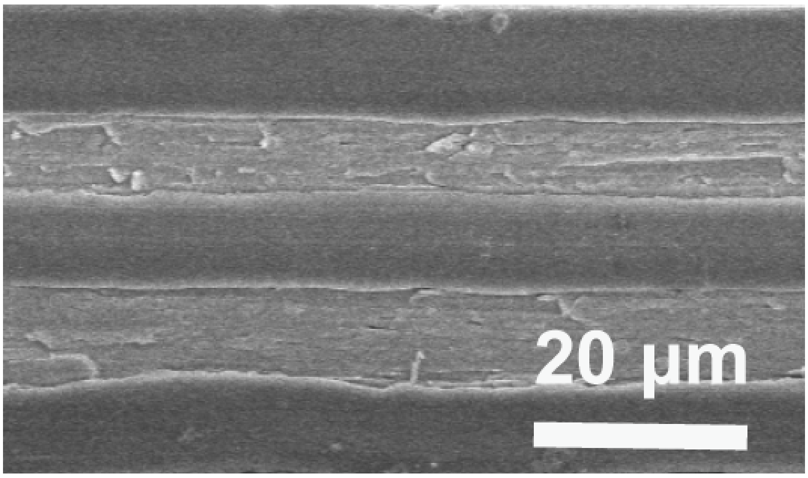

Fig. S46 SEM cross-section morphology of stacked multilayer films of electrodes and dielectric materials.

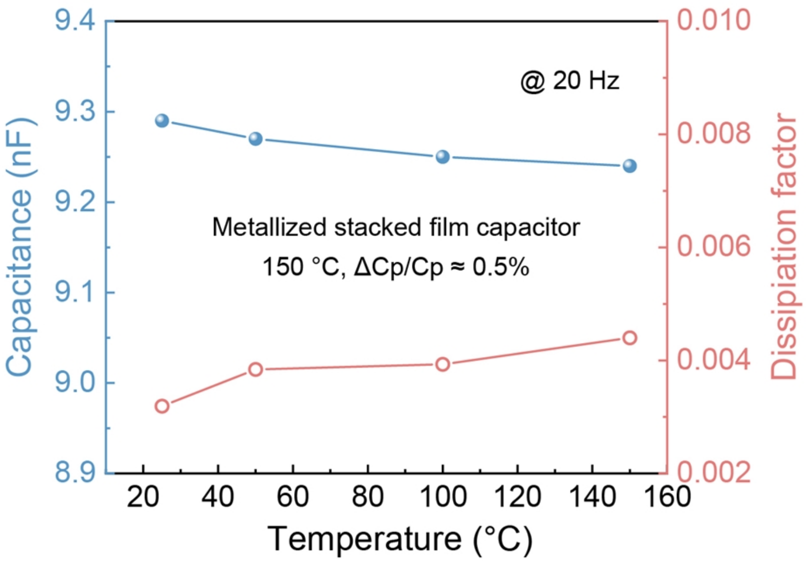

Fig. S47 Temperature-dependence of capacitance performance.

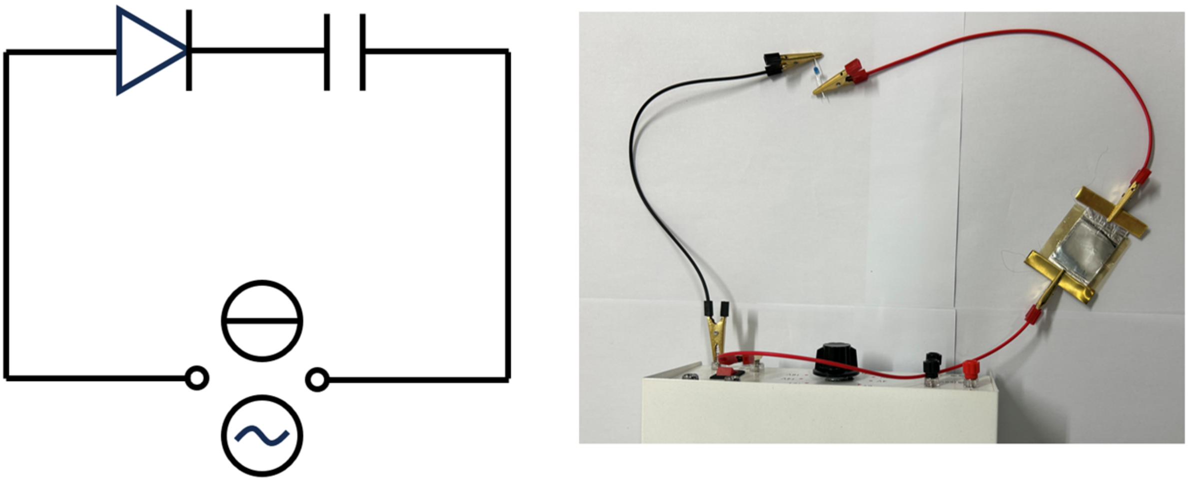

Fig. S48 Electrical circuit schematic of a capacitor operating under AC or DC voltage sources.

References

1. M. Frisch, *Inc, Wallingford CT*, 2013, **201**.
2. A. D. Becke, *Phys. rev. A*, 1988, **38**, 3098.
3. A. D. Becke, *J. Chem. Phys.*, 1992, **96**, 2155-2160.
4. T. Lu and S. Manzetti, *Stru. Chem.*, 2014, **25**, 1521-1533.
5. S. Manzetti and T. Lu, *J. Phys. Org. Chem.*, 2013, **26**, 473-483.
6. T. Lu and F. W. Chen, *J. Comput. Chem.*, 2012, **33**, 580-592.
7. Tian Lu, Molclus program, Version 1.12
8. E. Gross and W. Kohn, *Phys. Rev. Lett.*, 1985, **55**, 2850.
9. T. Yanai, D. P. Tew and N. C. Handy, *Chem. Phys. Lett.*, 2004, **393**, 51-57.